First publ. in: Journal of Organometallic Chemistry 694 (2009),5, pp. 655-666

Synthesis, solid state structure and spectro-electrochemistry of ferrocene-ethynyl phosphine and phosphine oxide transition metal complexes

Alexander Jakob [a], Petra Ecorchard [a], Michael Linseis [b], Rainer F. Winter [b], Heinrich Lang [a,*]

[a] Technische Universität Chemnitz, Fakultät für Naturwissenschaften, Institut für Chemie, Lehrstuhl für Anorganische Chemie, Straße der Nationen 62, 09111 Chemnitz, Germany
[b] Universität Regensburg, Institut für Anorganische Chemie, Universitätsstraße 31, 93040 Regensburg, Germany

The synthesis of ferrocene-ethynyl phosphine platinum dichloride complexes based on $(FcC{\equiv}C)_nPh_{3-n}P$ (**1a**, $n = 1$; **1b**, $n = 2$; **1c**, $n = 3$; Fc = ferrocenyl, $(\eta^5\text{-}C_5H_5)(\eta^5\text{-}C_5H_4)Fe$) is described. Air-oxidation of **1c** afforded $(FcC{\equiv}C)_3P{=}O$ (**6**). Treatment of **1a–1c** with $[(PhC{\equiv}N)_2PtCl_2]$ (**2**) or [(tht)AuCl] (tht = *tetra*hydro*th*iophene) (**7**), respectively, gave the heterometallic transition complexes *cis*-$[((FcC{\equiv}C)_nPh_{3-n}P)_2PtCl_2]$ (**3a**, $n = 1$; **3b**, $n = 2$; **3c**, $n = 3$) or $[((FcC{\equiv}C)_nPPh_{3-n})AuCl]$ (**8a**, $n = 1$; **8b**, $n = 2$). Further treatment of these molecules with $HC{\equiv}CMc$ (**4a**, Mc = Fc; **4b**, Mc = Rc = $(\eta^5\text{-}C_5H_5)(\eta^5\text{-}C_5H_4)Ru$) in the presence of [CuI] produced *trans*-$[((FcC{\equiv}C)Ph_2P)_2Pt(C{\equiv}CFc)_2]$ (**5**) (reaction of **3a** with **4a**) and $[(FcC{\equiv}C)_nPh_{3-n}PAuC{\equiv}CMc]$ ($n = 1$: **9a**, Mc = Fc; **9b**, Mc = Rc; $n = 2$: **11a**, Mc = Fc; **11b**, Mc = Rc) (reaction of **4a**, **4b** with **8a**, **8b**), respectively.

The structures of **3a**, **5**, **6**, **8**, **9a**, and **9b** in the solid state were established by single-crystal X-ray structure analysis. The main characteristic features of these molecules are the linear phosphorus–gold–acetylide arrangements, the tetra-coordination at phosphorus and the square-planar surrounding at platinum.

The electrochemical and spectro-electrochemical behavior of complexes **5**, **8a**, **9a**, **9b** and $[(Ph_3P)AuC{\equiv}CFc]$ was investigated in the UV/Vis/NIR. Near IR bands that are likely associated with charge transfer from the $((FcC{\equiv}C)Ph_2P)_2Pt$ or the $((FcC{\equiv}C)_nPh_{3-n}P)Au$ ($n = 0, 1$) moieties appear upon oxidation of the σ-bonded ferrocene-ethynyl groups. These bands undergo a (stepwise) blue shift as ferrocene-ethynyl substituents on the phosphine coligands are oxidized.

1. Introduction

Ferrocene is an exceptional building block to be incorporated in multimetallic transition metal complexes since it can act as a redox-label, one-electron reservoir and at the same time is a very robust compound [1]. Such assemblies provide interesting electronic, optical and/or magnetic properties [1,2]. One class of electron-rich sandwich complexes are ferrocenes containing exocyclic phosphine, phosphine chalcogenide or amine groups [3]. The electrochemically best studied candidate of this class of compounds is (diphenylphosphino)ferrocene, Ph_2PFc ($Fc = (\eta^5\text{-}C_5H_5)(\eta^5\text{-}C_5H_4)Fe$) [3]. Very recently, Kirss and Geiger reported about the anodic electrochemistry of phosphines and phosphine chalcogenides containing two or three ferrocenyl organometallic entities in weakly nucleophilic electrolytes [3]. In addition to the study of their redox behavior species of this kind are interesting building blocks for coordination compounds of higher nuclearity, due to the presence of the phosphine unit. Coordinative and/or covalent linking of such a modularly constructed sandwich building block allows the synthesis of heteromultimetallic ferrocenyl-containing assemblies in which the appropriate transition metal atoms are connected by carbon-rich organic and/or inorganic bridging moieties [4]. Promising members of this family of compounds are the (ferrocene-ethynyl)phosphines $(FcC{\equiv}C)_nPh_{3-n}P$ ($n = 1, 2, 3$), a hitherto only barely described class of molecules [5].

We report here on the synthesis, properties and the characterization of several platinum and gold (ferrocene-ethynyl)phosphine complexes. The spectro-electrochemical behavior of some trimetallic gold complexes and of a pentametallic platinum complex is also reported.

2. Results and discussion

The synthesis of transition metal complexes in which $(FcC{\equiv}C)_nPh_{3-n}P$ units (**1a**, $n = 1$; **1b**, $n = 2$; **1c**, $n = 3$) are connected to a $PtCl_2$ core, as given in *cis*-$[((FcC{\equiv}C)_nPh_{3-n}P)_2PtCl_2]$ ($n = 1$, **3a**; $n = 2$, **3b**; $n = 3$, **3c**), is presented in Scheme 1.

Reacting two equivalents of **1a–1c** with $[(PhC{\equiv}N)_2PtCl_2]$ (**2**) produced the multi(ferrocene-ethynyl)phosphine platinum(II)

* Corresponding author. Tel.: +49 371 531 21210; fax: +49 371 531 21219.
E-mail address: heinrich.lang@chemie.tu-chemnitz.de (H. Lang).

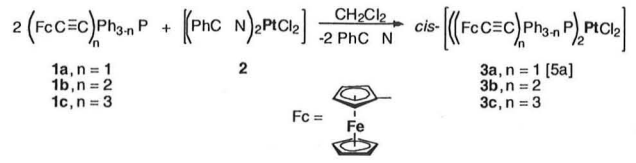

Scheme 1. Synthesis of phosphine platinum complexes **3a–3c**.

chlorides **3a–3c** in dichloromethane at ambient temperature in high yield. They can easily be isolated as analytically pure samples upon concentration of the reaction solutions and addition of petroleum ether, whereby the title compounds precipitate as orange solids. Single crystals of **3c** could be grown by diffusion of *n*-pentane into dichloromethane solutions containing **3c** at 25 °C.

The structure of **3c** in the solid state is depicted in Fig. 1. Relevant bond distances (Å) and angles (°) are listed in Table 1. The crystal and structure refinement data are presented in Table 6 (Section 4).

Complex **3c** crystallized in the monoclinic space group $P\bar{1}$. The structure of **3c** in the solid state shows a somewhat distorted square-planar coordination geometry at Pt1 with *cis*-oriented $(FcC{\equiv}C)_3P$ units (r.m.s. deviation of fitted atoms 0.0625 Å). The angles P1–Pt1–Cl2 and P2–Pt1–Cl1 in **3c** are almost linear at 175.58(4) and 173.35(4)°. The Pt–P and Pt–Cl separations (Fig. 1) agree well with those bond lengths reported for other chloro-phosphine platinum units in which the Pt–Cl bonds are likewise *trans* positioned to a phosphorus donor atom of high *trans*-influence [6]. The phosphorus–carbon distances (1.726(4)–1.752(4) Å) as well as the C≡C bond lengths (1.191(5)–1.198(5) Å) are in the typical range for this type of fragments [5,7]. As is characteristic of other ferrocene complexes the Fe–D separations (D = centroid of C_5H_5 and C_5H_4 units) range from 1.6406(2) to 1.6609(2) Å [8]. Based on the torsion angles C_{sp}–C_{Cp}–Fe–$C_{Cp'}$, whereby $C_{Cp'}$ was selected for the minimum resulting angle, eclipsed (torsion angle: C14–C15–Fe2–C20 = 7.7(4)°, C26–C27–Fe3–C32 = 8.5(4)°, C50–C51–Fe5–C56 = 9.0(4)°, and C62–C63–Fe6–C68 = 10.5(4)°) and staggered (torsion angle: C2–C3–Fe1–C8 = 20.8(4)° and C38–C39–Fe4–C44 = 18.6(4)°) conformations are typical.

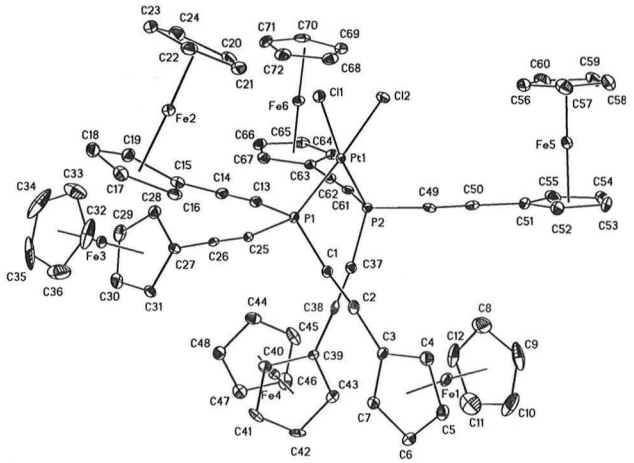

Fig. 1. ORTEP diagram (50% probability level) of **3c** with the atom-numbering scheme. (Hydrogen atoms are omitted for clarity.)

Table 1
Selected bond distances (Å) and angles (°) of complex **3c**.

Bond distances			
Pt1–Cl1	2.3362(10)	C13–C14	1.192(5)
Pt1–Cl2	2.3501(11)	C25–C26	1.198(5)
Pt1–P1	2.2152(11)	C37–C38	1.198(5)
Pt1–P2	2.2290(11)	C49–C50	1.191(5)
C1–C2	1.194(5)	C61–C62	1.192(5)
Bond angles			
P1–Pt1–Cl2	175.58(4)	Pt–P2–C61	112.38(14)
P2–Pt1–Cl1	173.35(4)	P1–C1–C2	174.6(4)
P1–Pt1–P2	93.85(4)	P1–C13–C14	169.8(4)
Pt1–P1–C1	115.28(14)	P1–C25–C26	167.6(4)
Pt1–P1–C13	118.50(14)	P2–C37–C38	173.3(4)
Pt1–P1–C25	110.74(14)	P2–C49–C50	172.3(4)
Pt1–P2–C37	118.25(14)	P2–C61–C62	171.7(4)
Pt–P2–C49	110.61(14)		

The ^1H, $^{13}C\{^1H\}$, $^{31}P\{^1H\}$ NMR and IR spectroscopic data are in agreement with the composition of the appropriate complexes and show no distinctive features compared with the systems discussed earlier (Section 4). The $J(^{31}P$–$^{195}Pt)$ coupling constants of 3760 (**3a**), 3886 (**3b**), and 4029 Hz (**3c**) found in the $^{31}P\{^1H\}$ NMR spectra confirm that *cis*-configurated platinum complexes were formed [5,9]. X-ray single-crystal structure determination of **3c** confirms this structural arrangement (vide supra).

Diphosphine platinum dichloride complexes are known to react with 1-alkynes to produce (bis)alkynyl complexes [10]. Thus, treatment of **3a** with an excess of HC≡CFc (**4a**) in the presence of [CuI] in a diisopropylamine solution produced with concomitant precipitation of $[H_2N^iPr_2]Cl$, orange *trans*-$[((FcC{\equiv}C)Ph_2P)_2Pt(C{\equiv}CFc)_2]$ (**5**) in a 75% isolated yield (Reaction (1)).

Most noteworthy in the IR spectrum of **5** is the appearance of two well-separated C≡C stretching bands at 2162 and 2180 cm^{-1} which can be assigned to the FcC≡CPt and $(FcC{\equiv}C)Ph_2P$ moieties (Section 4).

In the $^{31}P\{^1H\}$ NMR spectrum of **5** a sharp singlet is observed at −7.3 ppm. Due to the coupling of the ^{31}P nuclei with the ^{195}Pt isotope a $J(^{31}P$–$^{195}Pt)$ coupling constant of 2765 Hz is found, which proves that an isomerization from *cis*-**3a** to *trans*-**5** has taken place [11].

Single-crystal X-ray structure analysis was performed to confirm the molecular structure of **5** in the solid state. A view of this molecule is shown in Fig. 2, while selected bond distances (Å) and angles (°) are listed in Table 2. The crystal and structure refinement data are summarized in Table 6 (Section 4).

The platinum metal atom is held in a distorted square-planar environment (all atoms are perfectly in-plane) with the coordinated $(FcC{\equiv}C)Ph_2P$ units in a *trans*-position to each other (Fig. 2) which is in accord with findings for other bis(alkynyl) complexes of monodentate phosphines [12]. The platinum–carbon and platinum–phosphorus separations (Fig. 2) are within the range of reported Pt–P and Pt–C bonds [12]. In addition, the carbon–carbon distances of the appropriate acetylide ligands are typical of this type of structural building blocks (Fig. 2) [12].

While molecules **1a–1c** are fairly stable in the solid state, they slowly undergo oxidation at the phosphorus atom on exposure to air to give the respective phosphine oxides $(FcC{\equiv}C)_nPh_{3-n}P{=}O$ (Section 4). Due to the superior electron richness **1c** is easier oxidized than **1a** and **1b**. Phosphine **1c** is thus always contaminated with trace amounts of $(FcC{\equiv}C)_3P{=}O$ (**6**). This means that the more ferrocene-ethynyl moieties are present, the more reactive the complexes are. Heating **1c** in tetrahydrofuran and bubbling air

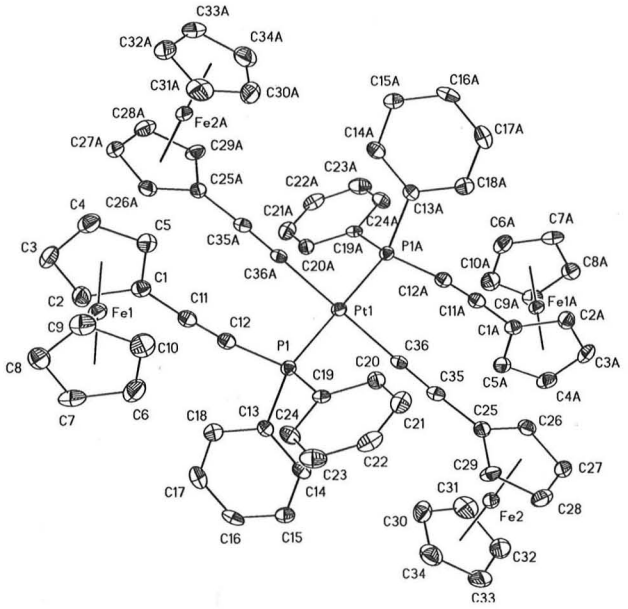

Fig. 2. ORTEP diagram (50% probability level) of **5** with the atom-numbering scheme. (Hydrogen atoms and the solvent molecule CH_2Cl_2 are omitted for clarity.)

Table 2
Selected bond distances (Å) and angles (°) of complexes **5** and **6**.

5		**6**	
Bond distances			
Pt1–P1	2.2923(9)	P1–O1	1.4685(16)
Pt1–C36	2.002(3)	P1–C12	1.7431(18)
P1–C12	1.753(4)	P1–C24	1.7537(19)
C11–C12	1.196(5)	P1–C36	1.7452(18)
C35–C36	1.203(5)	C11–C12	1.207(3)
		C23–C24	1.203(3)
		C35–C36	1.204(3)
Bond angles			
P1–Pt1–C36	89.08(10)	C11–C12–P1	171.17(16)
Pt1–P1–C12	115.66(12)	C23–C24–P1	177.32(17)
Pt1–P1–C13	114.99	C35–C36–P1	168.67(16)
Pt1–P1C19	116.60(12)	C12–P1–C24	103.38(8)
P1–C12–C11	1714(3)	C24–P1–C36	101.94(9)
C1–C11–C12	176.6(4)	C12–P1–C36	105.74(9)
Pt1–C36–C35	178.1(3)	C12–P1–O1	115.26(9)
C25–C35–C36	175.9(4)	C24–P1–O1	114.84(9)
		C36–P1–O1	114.18(9)

through the reaction solution gave orange **6** in quantitative yield (Reaction (2)).

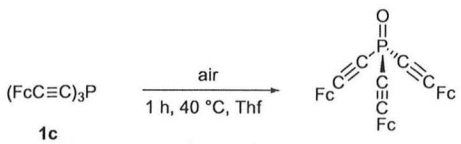

(2)

Compound **6** was characterized by elemental analysis, IR and NMR spectroscopy. Characteristic features in the IR spectrum of this compound are the C≡C stretching vibration at 2150 cm^{-1} and the $\nu_{(P=O)}$ absorption at 1254 cm^{-1} [13]. The progress of the oxidation of **1c** can be monitored by the disappearance of the ^{31}P NMR signal at −88.9 ppm (**1c**) [5] and the appearance of a new signal at lower field (−66.8 ppm). The key spectroscopic ^1H NMR feature is that the protons of the ferrocenyl C_5H_4 unit appear as two separated pseudo-triplets at ca. 4.3 and 4.6 ppm with J_{HH} coupling constants of 1.9 Hz. The resonance signal for the C_5H_5 protons is found at 4.25 ppm.

The identity of **6** was further confirmed by a single-crystal X-ray diffraction study. A view of the molecule is given in Fig. 3. Selected bond distances (Å) and angles (°) are given in Table 2, while the crystal and structure refinement data are presented in Table 6 (Section 4).

The overall structure of **6** is similar to those of related structurally characterized ethynyl-functionalized phosphines and ferrocenes with a pseudo-tetrahedral surrounding at the phosphorus atom [14]. Metrical parameters of molecule **6** are similar related to those reported previously for comparable molecules [14]. The phosphorus–carbon distances in **6** are 1.7431(18) (P1–C12), 1.7537(19) (P1–C24), and 1.7452(18) Å (P1–C36) indicating the higher *s* orbital contribution of the phosphorus–acetylide P–C bond, when compared with the $P–C_{phenyl}$ unit. The cyclopentadienyl rings are rotated by 8.62, 1.92 and 0.55° to each other which is in accord with an almost eclipsed conformation.

The ferrocene-ethynyl phosphine complexes **1a–1c** independently synthesized by Baumgartner et al. [5a] and our group, [5b] possess a lone pair of electrons at the phosphorus atom and hence, should coordinate to 14–16 valence electron complex fragments to form molecules of higher nuclearity. Exemplarily, trimetallic Fe–Au–M complexes (M = Fe, Ru) of composition [((FcC≡C)Ph_2P)AuC≡CMc] (**9a**, Mc = (η^5-C_5H_5)(η^5-C_5H_4)Fe; **9b**, Mc = (η^5-C_5H_5)(η^5-C_5H_4)Ru) were accessible in a consecutive reaction sequence by using (FcC≡C)Ph_2P (**1a**) as the key starting material (Scheme 2).

Compound **1a** reacts with [(tht)AuCl] (tht = *t*etra*h*ydro*t*hiophene) (**7**), whereby **1a** is added in a 25% excess in tetrahydrofuran at 0 °C to give **8a**. After column chromatography followed by crystallization from dichloromethane-*n*-pentane mixtures molecule **8a**

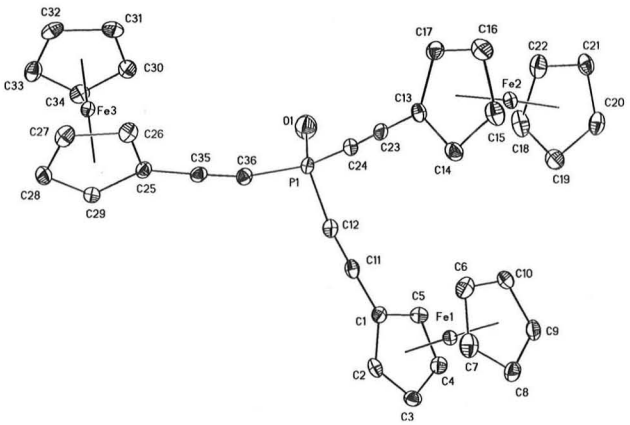

Fig. 3. ORTEP diagram (50% probability level) of **6** with the atom-numbering scheme. (Hydrogen atoms are omitted for clarity.)

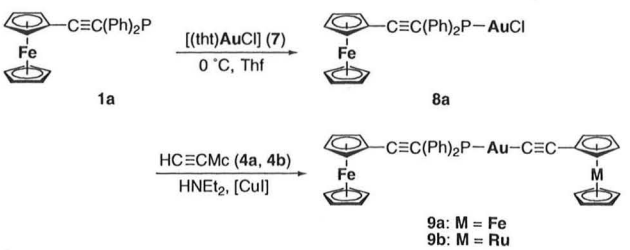

Scheme 2. Synthesis of **8a**, **9a**, and **9b** from **1a** (tht = *t*etra*h*ydro*t*hiophene).

could be isolated as an orange solid in 97% yield (Section 4). To introduce a further transition metal fragment, heterodimetallic **8a** was treated with HC≡CMc (**4a**, Mc = (η^5-C_5H_5)(η^5-C_5H_4)Fe; **4b**, Mc = (η^5-C_5H_5)(η^5-C_5H_4)Ru) in diethylamine as solvent and in the presence of catalytic amounts of [CuI] (Scheme 2). Following the methodology reported by Vicente et al. orange **9a** and **9b** were obtained in high yields [15].

Complexes **8a**, **9a**, and **9b** are, when compared with the starting material **1a**, more difficult to dissolve. Complexes **9a** and **9b**, for example, are only soluble in diethyl ether, tetrahydrofuran or dichloromethane.

The synthesis methodology used in the preparation of **9a** and **9b** should successfully be transferable to (FcC≡C)$_2$PhP (**1b**). Thus, this compound was subsequently reacted with [(tht)AuCl] (**7**) in a 25% excess of the phosphine to give the desired phosphine gold chloride coordination complex [((FcC≡C)$_2$PhP)AuCl] (**8b**) (Scheme 3). Treatment of the latter molecule with McC≡CH (**4a**, **4b**) produced [((FcC≡C)$_2$PhP)AuC≡CMc] (**11a**, Mc = (η^5-C_5H_5)(η^5-C_5H_4)Fe; **11b**, Mc = (η^5-C_5H_5)(η^5-C_5H_4)Ru). These compounds could, however, not be separated in pure form from the reaction mixtures.

The identities of **8a**, **8b**, **9a**, and **9b** have been confirmed by elemental analysis, IR, ^{1}H, ^{13}C{^{1}H}, and ^{31}P{^{1}H} NMR spectroscopy.

The consecutive preparation of higher nuclear heterometallic assemblies from **1a** and **1b** are confirmed by ^{1}H and ^{13}C{^{1}H} NMR spectroscopic studies, since after each individual synthesis step the newly introduced coordination or organometallic complex fragments can be detected (Section 4). The spectroscopic properties of all new complexes correlate with their formulation as di-, -tri- and tetrametallic transition metal systems showing the respective signal patterns for the organic units (Section 4).

The ^{31}P{^{1}H} NMR spectra of **8** and **9** indicate the presence of a single phosphorus environment with resonance signals at 1.9 (**8a**), ca. 15 (**9a**, **9b**), and −37.5 ppm (**8b**). A shift to lower field occurs upon coordination of the phosphorus atom to a AuCl moiety as given in **8a** and **8b** [16]. Replacing the chloride ligand in **8a** and **8b** by a C≡CMc unit results in a further downfield shift (Section 4) which is typical for phosphine gold(I) acetylides [16].

Most characteristic in the IR spectra of **8a**, **8b**, and **9a** is the appearance of only one C≡C stretching vibration at ca. 2155 cm^{-1} independent of the appropriate substitution pattern. However, this absorption is shifted to ca. 2167 cm^{-1} when the gold(I)-bonded FcC≡C unit is replaced by a ruthenocene acetylide moiety as given in **9b**. Only one $\nu_{C\equiv C}$ band was found for the two different alkynyl entities, PC≡CFc and AuC≡CFc, in the IR spectra of their coordination complexes.

In addition, the structures of **8a**, **9a**, and **9b** in the solid state were established by single X-ray structure analysis, thus confirming the assignments made from spectroscopic analysis. Suitable single crystals of **8a**, **9a**, and **9b** were obtained from slow vapor diffusion of *n*-pentane into a dichloromethane solution containing the appropriate transition metal complex at 25 °C. The molecular solid state structures of **8a**, **9a**, and **9b** are shown in Figs. 4–6, while selected bond lengths (Å) and angles (°) are given in Table 3. The crystal and structure refinement data for these species are presented in Table 7 (Section 4).

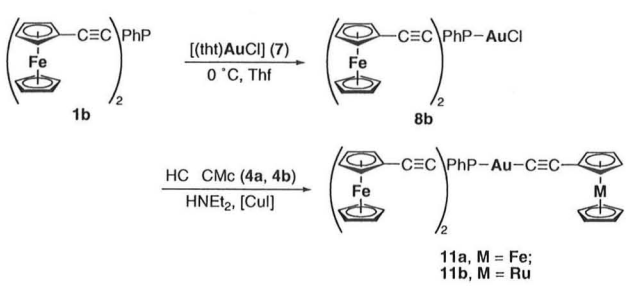

Scheme 3. Synthesis of heterobi- and -trimetallic **8b**, **11a**, and **11b**, respectively.

Complex **8a** crystallized in the monoclinic space group $P2_1/n$. The overall structural features of **8a** are similar to those of related (diphenyl)ferrocene-ethynyl phosphine and gold(I)–chloride-containing compounds with gold in a linear arrangement and phosphorus in a tetrahedral surrounding (Fig. 4). The cyclopentadienyl rings of the Fc entity are rotated by 5.8° showing an almost eclipsed conformation. The Au1–Cl1 and Au1–P1 distances agree well with this type of bonds. [17] The same is true for the P1–C12, P1–C13 and P1–C19 separations. The P1–C12 bond of 1.739(3) Å is expectedly shorter than the respective P1–C13 (1.815(3) Å) and P1–C19 (1.810(3) Å) distances (vide supra and Fig. 4) [17].

Molecules **9a** and **9b** crystallized in the monoclinic space groups $P2_1/c$ (**9a**) and $P2_1/a$ (**9b**). In both complexes the gold(I) ion adopts the usual linear coordination [18]. The phosphorus atom is tetra-coordinated, whereby two positions are occupied by phenyl groups and the third and fourth coordination sites are occupied by a C≡CFc and a AuC≡CFc (**9a**) or AuC≡CRc (**9b**) unit (Figs. 5 and 6). This coordination geometry is representative for phosphines coordinated to a transition metal complex fragment

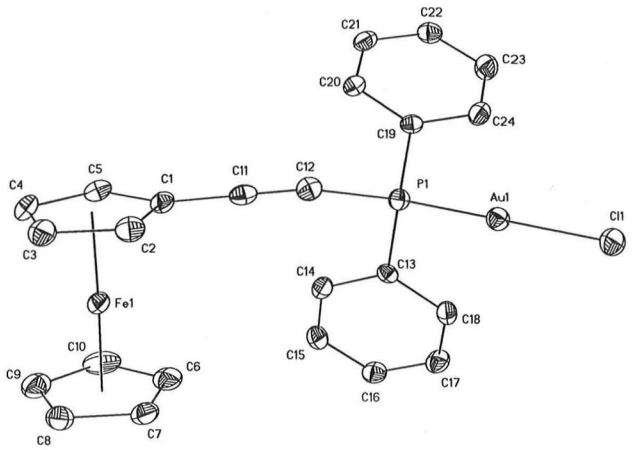

Fig. 4. ORTEP diagram (50% probability level) of **8a** with the atom-numbering scheme. (Hydrogen atoms are omitted for clarity.)

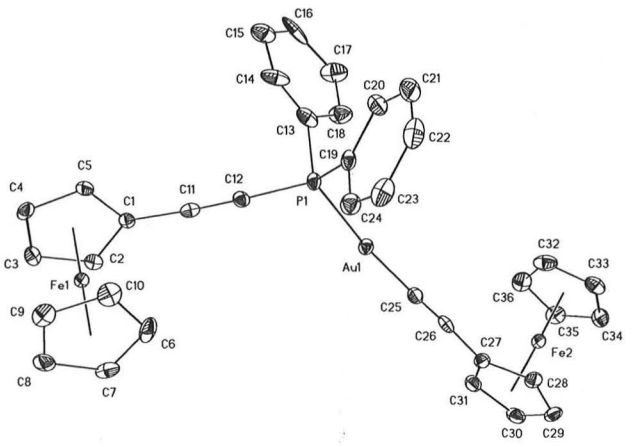

Fig. 5. ORTEP diagram (50% probability level) of **9a** with the atom-numbering scheme. (Hydrogen atoms are omitted for clarity.)

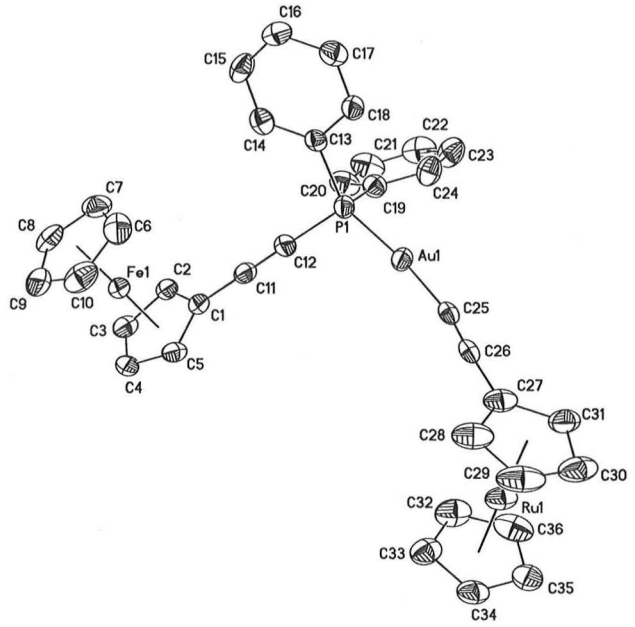

Fig. 6. ORTEP diagram (50% probability level) of **9b** with the atom-numbering scheme. (Hydrogen atoms and the solvent molecule dichloromethane are omitted for clarity.)

Table 3
Selected bond distances (Å) and angles (°) of complexes **8a**, **9a**, and **9b**.

	8a	9a	9b
Bond distances			
Au1–P1	2.2188(7)	2.2779(11)	2.2577(17)
Au–Cl1	2.2863(6)		
Au1–C25		2.000(5)	1.9841(19)
P1–C12	1.739(3)	1.753(4)	1.741(7)
P1–C13	1.815(3)	1.838(5)	1.833(7)
P1–C19	1.810(3)	1.821(4)	1.833(7)
C11–C12	1.202(4)	1.196(6)	1.196(9)
Bond angles			
C11–C12–P1	168.7(2)	176.8(4)	177.6(6)
P1–Au1–Cl1	179.68(2)		
P1–Au1–C25		174.24(12)	174.43(17)
C12–P1–C13	103.83(12)	104.2(2)	104.9(3)
C12–P1–C19	106.37(12)	103.8(2)	104.9(3)
C12–P1–Au1	114.35(9)	118.35(15)	110.0(2)
C13–P1–Au1	112.60(8)	110.39(17)	114.5(2)
C19–P1–Au1	114.83(9)	111.32(14)	116.4(2)
Au1–C25–C26		175.0(4)	169.6(5)

[16,18]. A comparison of the bond distances and bond angles in **9a** and **9b** shows that they are in the same range of reported assemblies featuring ferrocene-/ruthenocene-ethynyl, gold(I) alkynyl and PPh_2 building blocks (vide supra) [19].

Voltammetric measurements on complexes **5**, **8a**, **9a**, **9b** and of [$(Ph_3P)AuC{\equiv}CFc$] were performed in $CH_2Cl_2/[^nBu_4N]PF_6$ as the supporting electrolyte. Relevant data with potentials referenced against the ferrocene/ferrocenium couple [20,21] are collected in Table 4. Compounds [$(Ph_3P)AuC{\equiv}CFc$] and **8a** feature one, **9a** and **9b** two and **5** four redox-active metallocene-ethynyl moieties. Complex **8a** and [$(Ph_3P)AuC{\equiv}CFc$] help to establish the redox properties of the differently bonded ferrocene-ethynyl entities without possible interference from the other. Both complexes undergo a single reversible one-electron oxidation with a significantly lower oxidation potential for the gold-bonded ferrocene-ethynyl moiety (E_0 = −0.005 V for [$(Ph_3P)AuC{\equiv}CFc$]) compared to the phosphine-bonded one (E_0 = +0.350 V for **8a**, Fig. 7).

Table 4
Oxidation potentials of complexes [$(Ph_3P)AuC{\equiv}CFc$], **5**, **8a**, **9a**, and **9b**.[a]

Compound	E_0 in V against the [Fc/Fc^+] standard
[$(Ph_3P)AuC{\equiv}CFc$]	−0.005
5	−0.150 (1 e^-), −0.055 (1 e^-), 0.24 (2 e^-)
8a	−2.500, 0.350
9a	0.000, 0.260
9b	0.270[b] (2 e^-); 0.255[c]

[a] Voltammograms were recorded in $CH_2Cl_2/[^nBu_4N]PF_6$ (0.1 M) the supporting electrolyte.
[b] Partially reversible composite wave.
[c] At −78 °C.

Complex **9a** combines both types of ferrocene-ethynyl subunits (metal and phosphine-bonded) within the same molecule. As a consequence, it shows two reversible one-electron waves at half-wave potentials of 0.000 and +0.260 V vs. the ferrocene/ferrocenium standard (Fig. 8). With reference to [$(Ph_3P)AuC{\equiv}CFc$] and [$((FcC{\equiv}C)PPh_2)AuCl$] (**8a**), respectively, the first wave can be assigned to the gold-bonded ferrocene-ethynyl group and the second, more anodic one, to that of the $(FcC{\equiv}C)PPh_2$ ligand.

In contrast to **9a**, where a ferrocene-ethynyl unit is present, complex **9b** features a σ-bonded ruthenocene-ethynyl ligand. Ruthenocenes are generally more difficult to oxidize than their isostructural ferrocene counterparts. Their associated radical cations are highly electrophilic and readily react with even weak nucleophiles of the supporting electrolyte solution, which often renders their oxidation irreversible [22,23]. Thus, an anodic shift of the gold-bonded metallocene-ethynyl based oxidation wave is expected, when compared to **9a**. In fact, complex **9b** exhibits a partially reversible composite wave at +0.27 V which is followed by a broader, smaller and irreversible peak at E_p = +0.62 V (v = 0.1 V s^{-1}, Fig. 9a–c). Voltammograms recorded at v = 20 mV s^{-1} show that the main, less anodic wave comprises two separate electron transfer events as a shoulder appears on the rising part of the forward peak of the more anodic, reversible feature. Upon increasing the sweep rate the irreversible wave shifts anodically [24] to the point, where both features merge into a single, partially reversible composite wave with reverse-to-forward peak current ratios $i_{p,rev}/i_{p,f}$ in the range of 0.7–0.8 (Fig. 9a). With increasing sweep rate the overall reversibility of the composite wave increases, while the peak current ratio between the irreversible feature near 0.6 V and the main peak diminishes somewhat (Fig. 9b). Cooling to −78 °C renders the composite wave slightly more reversible and shifts its half-wave potential to +0.255 V but again without discernible resolution into separate features (Fig. 9c). This behavior can be interpreted by the reversible oxidation of the ferrocene-containing phosphine ligand and the partially reversible oxidation of the ruthenocene-ethynyl substituent, [25–27] which occur fortuitously at very similar potentials. The irreversible peak near 0.6 V arises from the further oxidation of the product that is formed on the chemical degradation of the oxidized ruthenocene-ethynyl moiety.

Complex **5** combines ferrocene-ethynyl substituents which are σ-bonded to a phosphorus as well as a platinum atom and hence, displays two pairs of reversible waves in the range of −0.2 to +0.3 V (Fig. 10a). The first pair of waves clearly consists of two overlapping, closely-spaced one-electron events that are resolved as individual peaks in square wave voltammetry (Fig. 10 b). Half-wave potentials as determined by deconvolution are −0.150 and −0.055 V. With reference to **8a**, **9a** and [$(Ph_3P)AuC{\equiv}CFc$] these waves can be assigned as the stepwise oxidation of the platinum-bonded ferrocene-ethynyl units. The oxidation of the

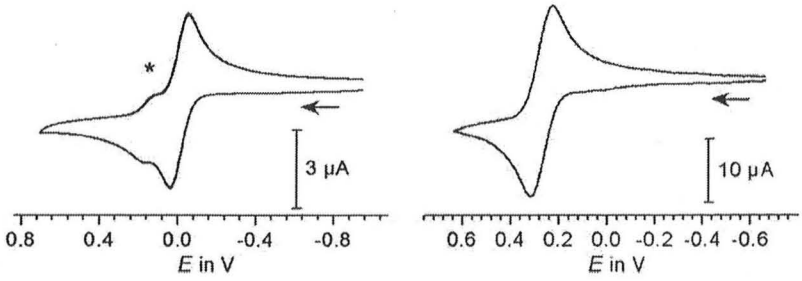

Fig. 7. Cyclic voltammograms of [(PPh_3)AuC≡CFc] (left) and **8a** (right) (10^{-3} M solution in dichloromethane at 25 °C with [$^nBu_4N$]PF_6 (0.1 M) as supporting electrolyte, scan rate 0.10 V s^{-1}). All potentials are referenced to the [FcH/FcH$^+$] redox couple (FcH = (η^5-C_5H_5)$_2$Fe) with E_0 = 0.00 V [24]. The wave indicated by the * symbol represents an impurity.

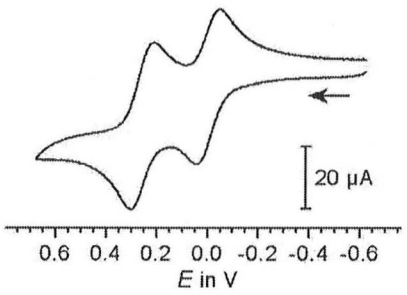

Fig. 8. Cyclic voltammogram of complex **9a** (10^{-3} M solution in dichloromethane at 25 °C with [$^nBu_4N$]PF_6 (0.1 M) as supporting electrolyte, scan rate 0.10 V s^{-1}). All potentials are referenced to the [FcH/FcH$^+$] redox couple (FcH = (η^5-C_5H_5)$_2$Fe) with E_0 = 0.00 V [24].

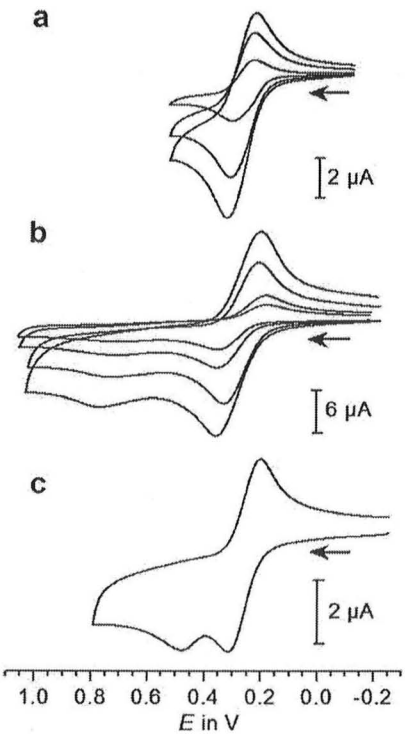

Fig. 9. Cyclic voltammograms of **9b**. (a) Scans over the first composite wave at sweep rates of 0.02, 0.1, and 0.2 V s^{-1} at 25 °C; (b) scans at 25 °C over a wider potential range to include the oxidation of the follow product at ν = 0.05, 0.2, 0.5, and 1.0 V s^{-1}; (c) scan at ν = 0.2 V s^{-1} after cooling to −78 °C (10^{-3} M solution in dichloromethane at 25 °C with [$^nBu_4N$]PF_6 (0.1 M) as supporting electrolyte). All potentials are referenced to the [FcH/FcH$^+$] redox couple (FcH = (η^5-C_5H_5)$_2$Fe) with E_0 = 0.00 V [24].

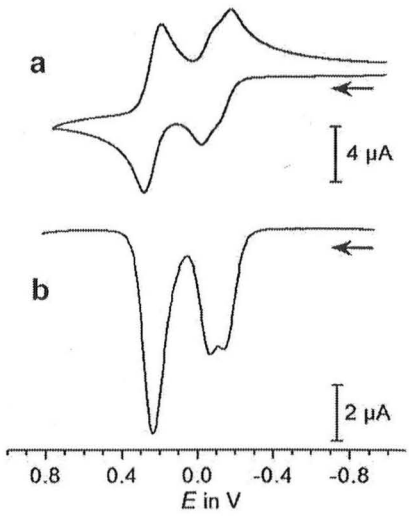

Fig. 10. (a) Cyclic voltammogram of complex **5** at ν = 0.1 V s^{-1}; (b) square wave voltammogram at ν = 25 Hz, step height = 4 mV (10^{-3} M solution in dichloromethane at 25 °C with [$^nBu_4N$]PF_6 (0.1 M) as supporting electrolyte). All potentials are referenced to the [FcH/FcH$^+$] redox couple (FcH = (η^5-C_5H_5)$_2$Fe) with E_0 = 0.00 V [24].

(FcC≡C)PPh_2 moieties, however, occurs as a single wave or peak at E_0 = +0.24 V with the net transfer of two-electrons.

Some findings to support the idea that electronic information is conjugatively transmitted along the π-conjugated MC≡CFc chain are: (i) The half-wave potentials of the ferrocene-ethynyl-based waves in [(Ph_3P)AuC≡CFc], **5** and **9a** are considerably lower than in parent ethynylferrocene (+0.16 V under our conditions) [28,29]. This reflects the electron donation by the σ-bonded ((FcC≡C)Ph_2P)$_2$Pt (**5**), (Ph_3P)Au or ((FcC≡C)Ph_2P)Au (**9a**) units. Similar observations have been reported for a variety of other heterobimetallic ferrocene-ethynyl complexes of platinum [30], gold [31], iron [22–33], and ruthenium [31,33–36]. (ii) The oxidation potential of **5** is lower than that in [(Tp^{ind})Ru(η^5-C_5(C_6H_4-4-C≡C-Pt(PEt_3)$_2$-C≡CFc)$_5$)] (0.15 V, Tp^{ind} = tris(indazolyl)borate) with a less electron donating alkynyl ligand *trans* to the ferrocene-ethynyl moiety [37] but close to complexes *trans*-[Pt(C≡CFc)(C_6H_4-4-X)(PPh_3)$_2$] (X = H, Me, OMe, Cl, COMe, CO_2Me) [30,38] and *trans*- [(Ph_3P)$_2$Pt(C≡CFc)$_2$] (−0.07 and 0.19 V), respectively [38].

Previous work on heterobimetallic complexes of type [MC≡CMc]$^+$ (Mc = Fc, Rc) featuring σ-bonded metallocene-ethynyl moieties has disclosed that their singly oxidized radical cations generally display characteristic low energy absorptions in the visible or in the near infrared that are associated with the transfer of electron density from the reduced electron-rich M donor to the

Table 5
Deconvoluted band maxima for [(Ph$_3$P)AuC≡CFc], **5**, **9a**, and **9b** in their various oxidation states.

Compound	λ_{max} in nm according to spectral deconvolution[a]
[(Ph$_3$P)AuC≡CFc]	446, 356, 334
[(Ph$_3$P)AuC≡CFc$^+$]	855, 755, 560, 500, 410
9a	480, 440, 356, 322
[9a]$^{\cdot+}$	850, 760, 560, 500, 415
[9a]$^{2+}$	805, 700, 560, 460
9b	470, 425, 360, 317
[9b]$^{2+}$	700, 605, 475, 408
5	470, 422, 386, 333
[5]$^{\cdot+}$	1013, 444, 329
[5]$^{2+}$	975, 885, 575, 452, 360
[5]$^{4+}$	951, 755, 572, 450, 360

[a] Similarly good fits were obtained with somewhat different parameter sets. The error in λ_{max} is ±5 nm for the higher and ±10 nm for the lower energy absorption of the oxidized forms.

oxidized Mc$^+$ acceptor site [28,30,32,34–37,39]. We have probed for the occurrence of similar bands in [(Ph$_3$P)AuC≡CFc] and **9a**, **9b**, and **5** by means of *in situ* UV/Vis/NIR spectro-electrochemistry. The results of these investigations are summarized in Table 5. Besides the intense $n \rightarrow \pi^*$ and $\pi \rightarrow \pi^*$ type transitions of the ferrocenyl and the Ph$_3$P moieties in the UV, compound [(Ph$_3$P)AuC≡CFc] has a weaker, broad and asymmetric electronic absorption peaking at 446 nm associated with the AuC≡CFc moiety. Oxidation of the ferrocene-ethynyl moiety induces the growth of a new composite low energy absorption band with (deconvoluted) peak maxima of 855 and 755 nm and band widths of about 1550 and 2550 cm^{-1}. Higher energy absorptions include weaker bands at 560 and 500 nm and a stronger absorption at 410 nm (Fig. 11).

The spectra of neutral **9a** and of monooxidized **[9a]$^{\cdot+}$** with the same oxidized Fc$^+$C≡CAu unit as in [(Ph$_3$P)AuC≡CFc]$^+$ closely resemble the ones observed for the simpler PPh$_3$ ligated compound in its respective oxidation state (Table 5, Fig. 12a) with a composite low-energy band with deconvoluted peak maxima of 850 and 760 nm, weaker bands at 560 and 500 nm and a stronger absorption at 415 nm. Upon the second, (FcC≡C)Ph$_2$P-based oxidation to **[9a]$^{2+}$** the low energy bands intensify and experience a blue shift of about 700 and 900 cm^{-1} to 805 and 700 nm (Fig. 12b). This blue shift probably reflects the lowering of the ((FcC≡C)Ph$_2$P)Au-based donor orbitals as a consequence of the oxidation of the (FcC≡C)Ph$_2$P ligand. The latter event is expected to increase the energy of the (RPh$_2$P)Au → C≡CFc$^+$ charge-transfer (CT) transition.

The ruthenocene analog **9b**, despite its only partially reversible behavior in cyclic voltammetry, gave still useful results under the thin-layer conditions of *in situ* spectro-electrochemistry. Spectra obtained after a full oxidation/reduction cycle were very similar to those of pristine **9b**. Characteristic bands of oxidized **9b** (which is probably present as **[9b]$^{2+}$**) appear at 700 and 605 nm, and thus at higher energies as in the ferrocene-ethynyl counterpart **[9a]$^{2+}$**. These differences may relate to the well-known propensity of oxidized ruthenocene-ethynyls to rearrange to cyclopentadienylidene type structures [25–27].

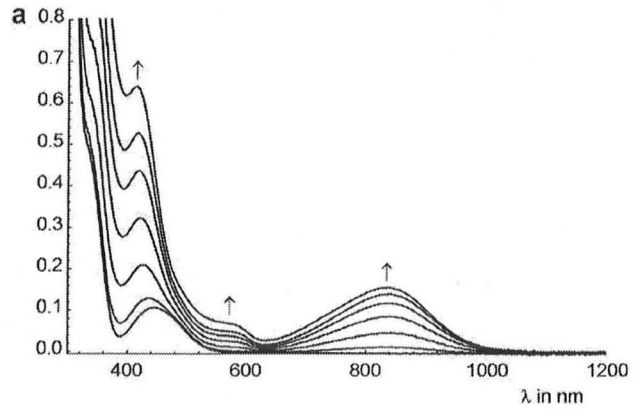

Fig. 11. Spectroscopic changes upon oxidation of [(Ph$_3$P)AuC≡CFc] (1,2-C$_2$H$_4$Cl$_2$/["Bu$_4$N]PF$_6$) in an OTTLE cell.

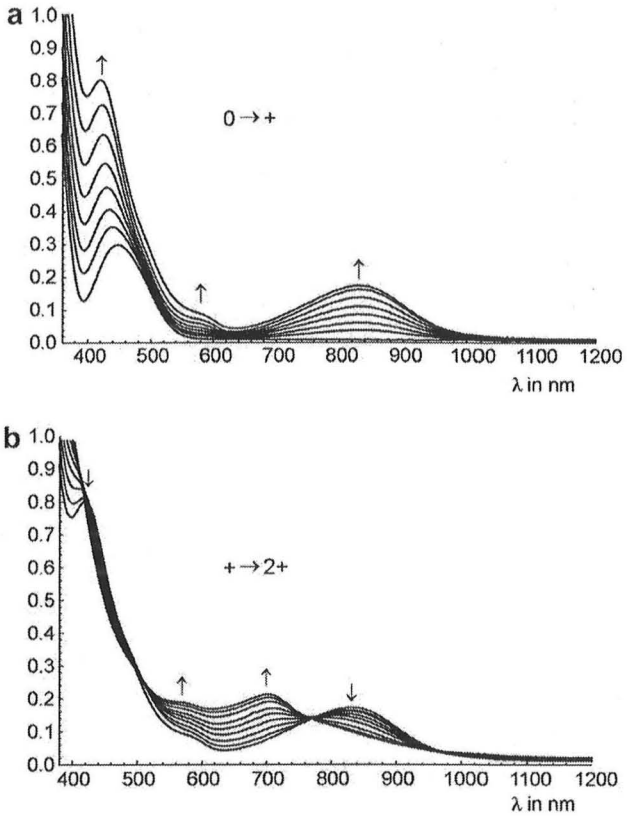

Fig. 12. Spectroscopic changes upon stepwise oxidation of **9a** (1,2-C$_2$H$_4$Cl$_2$/["Bu$_4$N]PF$_6$) in an OTTLE cell. (a) Spectroscopic changes upon the first oxidation to **[9a]$^{\cdot+}$**, (b) the second oxidation to **[9a]$^{2+}$**.

The resolved, stepwise oxidations of the platinum-bonded C≡CFc moieties of complex **5** raise the question whether they are electronically coupled across the platinum center or not. While (R$_3$P)$_2$Pt entities are usually regarded as insulating [30,40,41], some accounts of π-delocalization along the RC≡C–Pt–C≡CR axis in *trans*-dialkynyl platinum complexes have already appeared [38,39,42–44].

Such an "electronic coupling" should give rise to a low-energy absorption band at the mixed-valent **[5]$^{\cdot+}$** state but not in the bordering **5** and **[5]$^{2+}$** states, where *both* C≡CFc moieties are present in either their reduced or oxidized states. The analysis of the electronic spectra of **[5]$^{\cdot+}$** is, however, complicated by the proximity of the two PtC≡CFc-based oxidation waves. The 0.095 V splitting of half-wave potentials translates via Eq. (1) into a comproportionation constant of 40 for the intermediate mono-cation. In Eq. (3), n denotes the number of transferred electrons, F is Faraday's constant, and R and T have their usual meaning.

$$[5]^{2+} + [5] \rightleftarrows 2[5]^{+};\ K_{comp} = \exp[n \cdot F \cdot \Delta E_0/(R \cdot T)] \quad (3)$$

In such a constellation, spectra recorded at any stage during the first two oxidations represent mixtures of neutral **5**, monoxidized **[5]$^{\cdot+}$** and **[5]$^{2+}$** (Fig. 13a and b). From the spectra of neutral **5** and

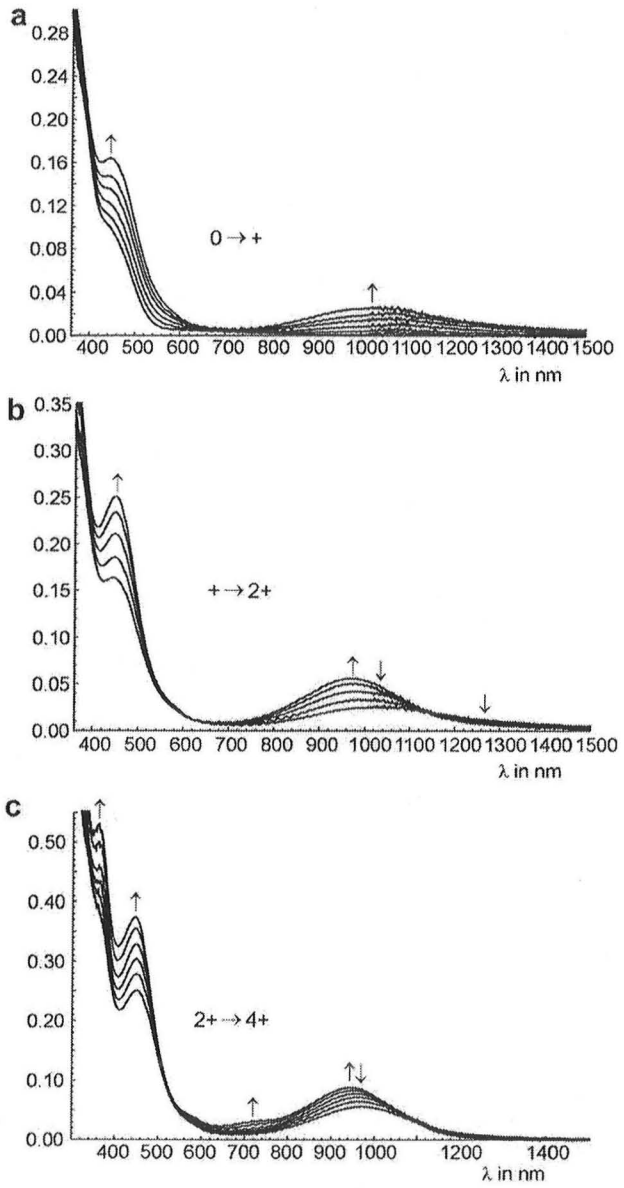

Fig. 13. Spectroscopic changes upon stepwise oxidation of **5** (1,2-$C_2H_4Cl_2$/[$^nBu_4N$]PF_6) in an OTTLE cell. (a) Spectroscopic changes upon the first oxidation to $[\mathbf{5}]^{\cdot+}$, (b) the second oxidation to $[\mathbf{5}]^{2+}$and (c) the third oxidation to $[\mathbf{5}]^{4+}$.

dioxidized $[\mathbf{5}]^{2+}$ and from the value of the comproportionation constant K_{comp} the spectrum of $[\mathbf{5}]^{\cdot+}$ can be calculated. It is given as Fig. 14. The low energy portion of the spectrum is adequately simulated by a single band peaking at 1013 nm. Given the general appearance of low energy absorptions in every complex with a metal-bonded oxidized C≡CFc$^+$ moiety, we assign this band to the Pt → C≡CFc$^+$ charge transfer transition. The absence of any discernible FcC≡C → FcC≡C$^+$ intervalence charge transfer band characterizes $[\mathbf{5}]^{\cdot+}$ as a localized mixed-valent system [45].

In analogy to complex **9a** and in further keeping with the Pt → C≡CFc$^+$ assignment, the 1013 nm band of $[\mathbf{5}]^{\cdot+}$ undergoes a stepwise blue shift with a concomitant increase in overall intensity as further ferrocene tags are oxidized ($[\mathbf{5}]^{\cdot+} \rightarrow [\mathbf{5}]^{2+}$, $[\mathbf{5}]^{2+} \rightarrow [\mathbf{5}]^{4+}$, Fig. 13b and c). For both, $[\mathbf{5}]^{2+}$ and $[\mathbf{5}]^{4+}$, the band envelope is notably asymmetric and requires the inclusion of two separate absorptions in the deconvolution procedure (see Table 5).

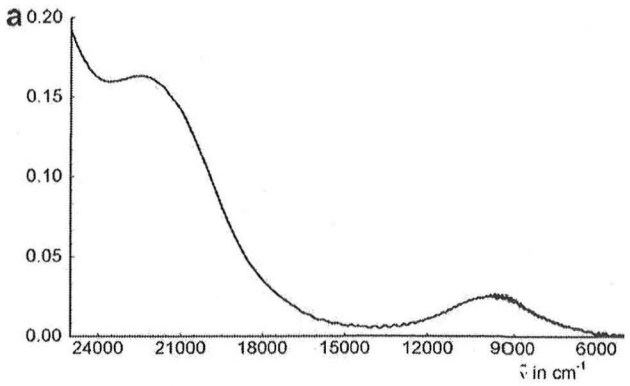

Fig. 14. Calculated spectrum of singly oxidized $[\mathbf{5}]^{\cdot+}$.

According to Eq. (4), the band maximum of a charge transfer band in a heterobimetallic, (formally) mixed-valent system depends on the redox asymmetry between the dislike redox sites. This is expressed by the energy difference ΔG° between the different valence tautomers (MC≡CFc$^+$ and M$^+$C≡CFc), while λ represents the reorganization energy. Further examples within the context of MC≡CMc$^+$ systems have been reported by Sato et al. [30,32,36,39].

$$\tilde{\nu}_{max} = \lambda + \Delta G^\circ \qquad (4)$$

The blue shift of the relevant low-energy absorption band upon replacement of Pt(PPh_3)$_2$(C≡CFc^{n+}) (n = 0, **5**; n = 1: $[\mathbf{5}]^{\cdot+}$) by Au(PR_2R') moieties (R' = Ph or C≡CFc^{n+} (n = 0, $[\mathbf{9a}]^{\cdot+}$; n = 1: $[\mathbf{9a}]^{2+}$) and upon the oxidation of ferrocene-ethynyl substituents at the phosphine co-ligand is understandable on that basis. Also pertinent to the systems in the current study are complexes *trans*-[FcC≡CPt(PPh_3)$_2$(C_6H_4-4-X)], where the PtC≡CFc$^+$ band systematically blue shifts as the σ_p^+ parameter of the *para*-substituent X increases. [30] Our value of 9870 cm^{-1} (1013 nm) for $[\mathbf{5}]^{\cdot+}$ slightly exceeds those observed for the above aryl complexes (9300–9480 cm^{-1}). The [(FcC≡C)Ph_2P)$_2$Pt(C≡CFc)] entity thus appears to be slightly less electron donating than [Pt(PPh_3)$_2$(C_6H_4-(-4-COMe))], while the (Ph_3P)Au and ((FcC≡C)Ph_2P)Au entities are even weaker donors. This also matches the trends in the oxidation potentials of the metal bonded FcC≡C subunit (Table 4).

3. Conclusion

Different synthesis methods for the preparation of ferrocene-ethynyl phosphine and phosphine oxide transition metal complexes of structural type (FcC≡C)$_3$P=O, [((FcC≡C)$_n$$Ph_{3-n}$P)AuCl] ($n$ = 1, 2), [((FcC≡C)Ph_2P)AuC≡CMc], [((FcC≡C)$_n$$Ph_{3-n}$P)AuC ≡CMc] ($n$ = 1, 2), *cis*-[((FcC≡C)$_n$$Ph_{3-n}$P)$_2$$PtCl_2$] and *trans*-[((FcC≡C)$Ph_2$P)$_2$Pt(C≡CFc)$_2$] (Mc=Fc, Rc; Fc = ($\eta^5$-$C_5H_5$)($\eta^5$-$C_5H_4$)Fe; Rc = ($\eta^5$-$C_5H_5$)($\eta^5$-$C_5H_4$)Ru) are reported. In these species ferrocene and/or ruthenocene sandwich units are interconnected by ethynyl phosphine and metal-ethynyl bridging units. Electrochemical studies show chemically reversible oxidations of the metal and phosphine-bonded FcC≡C moieties. The half-wave potentials of these processes respond to the electron density at the heterometal moiety. Upon oxidation of the σ-bonded McC≡C entities low energy absorption bands appear in the near infrared that are likely associated with the transfer of charge from the heterometal atom M to C≡CMc$^+$. These bands show the expected blue shift as M becomes less electron donating, i.e., as the redox asymmetry between the M and FcC≡C redox sites increases. Our results also argue against any "electronic coupling" between the oxidized Fc$^+$ and the reduced Fc site across the –C≡C–Pt(PPh_2(C≡CFc))$_2$–C≡C– linker in mono-oxidized $[\mathbf{5}]^{\cdot+}$ despite the 95 mV splitting of redox potentials.

4. Experimental

4.1. General data

All reactions were carried out under an atmosphere of nitrogen using standard Schlenk techniques. Tetrahydrofuran, diethyl ether, *n*-hexane and *n*-pentane were purified by distillation from sodium/benzophenone ketyl; dichloromethane was purified by distillation from calcium hydride. Celite (purified and annealed, Erg. B.6, Riedel de Haen) was used for filtrations.

4.2. Instruments

Infrared spectra were recorded with a Perkin–Elmer FT-IR spectrometer Spectrum 1000. ^{1}H NMR spectra were recorded with a Bruker Avance 250 spectrometer operating at 250.130 MHz in the Fourier transform mode; $^{13}C\{^1H\}$ NMR spectra were recorded at 62.860 MHz. Chemical shifts are reported in δ units (parts per million) downfield from tetramethylsilane with the solvent as reference signal (^{1}H NMR: $CDCl_3$ (99.8%), $\delta = 7.26$; $(CD_3)_2CO$ (99.9%), $\delta = 2.05$; CD_3CN (99.8%), $\delta = 1.94$. $^{13}C\{^1H\}$ NMR: $CDCl_3$ (99.8%), $\delta = 77.16$; $(CD_3)_2CO$ (99.9%), $\delta = 29.84$, 206.26). The abbreviation pt in the ^{1}H NMR spectra corresponds to pseudo-triplet. Cyclic voltammograms were recorded in a dried cell purged with purified argon. Platinum wires served as working electrode and counter electrode. A saturated calomel electrode in a separated compartment or a silver wire served as (pseudo)reference electrode. In the latter case, potential calibration was done by addition of ferrocene to the analyte solution. All electrode potentials are converted using the redox potential of the ferrocene–ferrocenium couple [FcH/FcH$^+$] (FcH = $(\eta^5\text{-}C_5H_5)_2Fe$, $E_0 = 0.00$ V, [20,21] as reference. Electrolyte solutions were prepared from tetrahydrofuran (for **5**) or dichloromethane (for **9a** and **9b**) and $[^nBu_4N]PF_6$ (Fluka, dried in *oil-pump* vacuum). The respective organometallic complexes were added at $c = 1.0$ mM. Cyclic voltammograms were recorded using a Voltalab 3.1 potentiostat (Radiometer) equipped with a digital electrochemical analyzer DEA 101 and an electrochemical interface IMT 102 or a BAS CV 50 instrument. Spectro-electrochemistry was performed in a home-built optically transparent thin-layer electrolysis (OTTLE) cell following the design of Hartl and coworkers [46]. Melting points were determined using analytically pure samples, sealed off in nitrogen purged capillaries on a Gallenkamp MFB 595 010 M melting point apparatus. Microanalyses were performed by the Institute of Organic Chemistry, Chemnitz, University of Technology and by the Institute of Organic Chemistry, University of Heidelberg.

4.3. Reagents

FcC≡CH [47a], RcC≡CH [47b], $[(PhC{\equiv}N)_2PtCl_2]$ [48], [(tht)AuCl] [49], and $(FcC{\equiv}C)_nPh_{3-n}P$ ($n = 1, 2, 3$) [5b] were prepared according to published procedures. All other chemicals were purchased by commercial suppliers and were used without further purification.

4.4. Synthesis of cis-[(FcC≡C)Ph$_2$P)$_2$PtCl$_2$] (**3a**)

One hundred milligrams (0.21 mmol) of $[(PhC{\equiv}N)_2PtCl_2]$ (**2**) and 167 mg (0.42 mmol) of $(FcC{\equiv}C)Ph_2P$ (**1a**) were dissolved in 40 mL of dichloromethane and were stirred for 1 h at 25 °C. Afterward the reaction solution was reduced in volume under reduced pressure and the orange title compound was precipitated by addition of petroleum ether. Yield: 190 mg (0.18 mmol, 85% based **2**).

Anal. Calc. for $C_{48}H_{38}Cl_2Fe_2P_2Pt$ (1053.02): C, 54.70; H, 3.64. Found: C, 54.23; H, 3.65%. M.p.: 216 °C (decomp.). IR (KBr, cm^{-1}): 2159 (s, $\nu_{C\equiv C}$). ^{1}H NMR (δ, $CDCl_3$): 4.04 (s, 10H, C_5H_5), 4.16 (pt, $J_{HH} = 1.9$ Hz, H^β/C_5H_4), 4.21 (pt, $J_{HH} = 1.7$ Hz, H^α/C_5H_4), 7.35–7.53 (m, 12H, C_6H_5), 7.81–7.97 (m, 8H, C_6H_5). $^{13}C\{^1H\}$ NMR (δ, $CDCl_3$): 61.3 (C^i/C_5H_4), 70.0 (C^β/C_5H_4), 70.2 (C_5H_5), 72.8 (C^α/C_5H_4), 111.0 (C/C≡C), 128.3 (d, $J_{CP} = 6.4$ Hz C^m/C_6H_5), 129.3 (d, $J_{CP} = 77.4$ Hz, C^i/C_6H_5), 131.3 (C^p/C_6H_5), 133.8 (pt, $J_{CP} = 6.1$ Hz, C^o/C_6H_5). $^{31}P\{^1H\}$ NMR (δ, $CDCl_3$): -12.1 ($J_{^{31}P^{195}Pt} = 3760$ Hz).

4.5. Synthesis of cis-[((FcC≡C)$_2$PhP)$_2$PtCl$_2$] (**3b**)

Complex **3b** was synthesized on a similar manner as discussed for **3a**: 70 mg (0.15 mmol) of $[(PhC{\equiv}N)_2PtCl_2]$ (**2**), 156 mg (0.30 mmol) of $(FcC{\equiv}C)_2PhP$ (**1b**). After appropriate work-up, complex **3b** was obtained as an orange solid. Yield: 180 mg (0.14 mmol, 92% based on **2**).

Anal. Calc. for $C_{60}H_{48}Cl_2Fe_4P_2Pt$ (1318.97): C, 54.59; H, 3.67. Found: C, 54.23; H, 3.65%. M.p.: 146 °C (decomp.). IR (KBr, cm^{-1}): 2158 (s, $\nu_{C\equiv C}$). **^{1}H NMR** (δ, $CDCl_3$): 4.20 (s, 20H, C_5H_5), 4.25 (pt, $J_{HH} = 1.9$ Hz, 8H, H^β/C_5H_4), 4.41 (pdq, $J_{HH} = 11.6$ Hz, $J_{HH} = 1.4$ Hz, $J_{HH} = 1.9$ Hz, 8H, H^α/C_5H_4), 7.45–7.59 (m, 6H, C_6H_5), 8.18–8.32 (m, 4H, C_6H_5). $^{13}C\{^1H\}$ NMR (δ, $CDCl_3$): 61.4 (C^i/C_5H_4), 70.1 (C^β/C_5H_4), 70.5 (C_5H_5), 72.5 (C^α/C_5H_4), 128.7 (d, $J_{CP} = 7.1$ Hz, C^m/C_6H_5), 128.9 (C^i/C_6H_5), 131.8 (C^p/C_6H_5), 133.4 (pt, $J_{CP} = 7.4$ Hz, C^o/C_6H_5). $^{31}P\{^1H\}$ NMR (δ, $CDCl_3$): −43.2 ($J_{^{31}P^{195}Pt} = 3886$ Hz).

4.6. Synthesis of cis-[((FcC≡C)$_3$P)$_2$PtCl$_2$] (**3c**)

Complex **3c** was synthesized in a similar manner as described for **3a**: 165 mg (0.35 mmol) of $[(PhC{\equiv}N)_2PtCl_2]$ (**2**), 460 mg (0.70 mmol) of $(FcC{\equiv}C)_3P$ (**1c**). After appropriate work-up, complex **3c** was isolated as an orange solid. Yield: 515 mg (0.33 mmol, 93% based on **2**).

Anal. Calc. for $C_{72}H_{54}Cl_2Fe_6P_2Pt$ (1580.88): C, 54.65; H, 3.44. Found: C, 54.41; H, 3.34%. M.p.: 135 °C (decomp.). IR (KBr, cm^{-1}): 2156 (s, $\nu_{C\equiv C}$). ^{1}H NMR (δ, $CDCl_3$): 4.29 (pt, $J_{HH} = 1.9$ Hz, 12H, H^β/C_5H_4), 4.30 (s, 30H, C_5H_5), 4.61 (pt, $J_{HH} = 1.9$ Hz, 12 H, H^α/C_5H_4). $^{13}C\{^1H\}$ NMR (δ, $CDCl_3$): 61.2 (C^i/C_5H_4), 70.3 (C^β/C_5H_4), 70.8 (C^α/C_5H_4), 72.7 (C_5H_5). $^{31}P\{^1H\}$ NMR (δ, $CDCl_3$): −77.1 ($J_{^{31}P^{195}Pt} = 4029$ Hz).

4.7. Synthesis of trans-[((FcC≡C)Ph$_2$P)$_2$Pt(C≡CFc)$_2$] (**5**)

To 170 mg (0.16 mmol) of $[(FcC{\equiv}CPh_2P)_2PtCl_2]$ (**3a**) and 67 mg (0.32 mmol) of ethynylferrocene (**4a**) dissolved in 40 mL of diisopropylamine was added 1 mg of [CuI]. After 1 day of stirring, all volatiles were removed in *oil-pump* vacuum and the orange residue was chromatographed on alumina with dichloromethane/*n*-hexane (1:1, vs/vs) as eluent. Complex **6** was isolated as an orange solid. Yield: 170 mg (0.12 mmol, 75% based on **3a**).

Anal. Calc. for $C_{72}H_{56}Fe_4P_2Pt \times 1/3CH_2Cl_2$ (1427.10): C, 60.76; H, 3.99. Found: C, 60.79; H, 4.15%. M.p.: 198 °C (decomp.). IR (KBr, cm^{-1}): 2180 (m, $\nu_{PtC\equiv C}$), 2162 (m, $\nu_{PC\equiv C}$). ^{1}H NMR (δ, $CDCl_3$): 3.81 (pt, $J_{HH} = 1.7$ Hz, 4H, $H^\beta C_5H_4$/FcC≡CPt), 3.84 (s, 10H, C_5H_5/FcC≡CPt), 3.86 (pt, $J_{HH} = 1.7$ Hz, 4H, $H^\alpha C_5H_4$/FcC≡CPt), 4.19 (s, 10H, C_5H_5/FcC≡CP), 4.23 (pt, $J_{HH} = 1.9$ Hz, 4H, H^β/C_5H_4/FcC≡CP), 4.55 (pt, $J_{HH} = 1.9$ Hz, 4H, H^α/C_5H_4/FcC≡CP), 5.29 (s, CH_2Cl_2), 7.44–7.50 (m, 12H, C_6H_5), 8.08–8.19 (m, 8H, C_6H_5). $^{31}P\{^1H\}$ NMR (δ, $CDCl_3$): −7.3 ($J_{^{31}P^{195}Pt} = 2765$).

4.8. Synthesis of (FcC≡C)$_3$P=O (**6**)

Through a solution of 40 mL tetrahydrofuran containing 100 mg (0.15 mmol) of $(FcC{\equiv}C)_3P$ (**1c**) was bubbled air for 1 h at 40 °C. After evaporation of the solvent in *oil-pump* vacuum, the title compound was obtained as a red-orange solid. Yield: 101 mg (0.15 mmol, 99% based on **1c**).

Anal. Calc. for $C_{36}H_{27}Fe_3PO$ (673.99): C, 64.10; H, 4.04. Found: C, 64.14; H, 4.23%. M.p.: 178 °C (decomp.). IR (KBr, cm^{-1}): 2151 (s, $\nu_{C\equiv C}$), 1254 (w, $\nu_{P=O}$). ^1H NMR (δ, $CDCl_3$): 4.32 (s, 15H, C_5H_5), 4.34 (pt, J_{HH} = 1.7 Hz, 6H, H^{β}/C_5H_4), 4.65 (pt, J_{HH} = 1.7 Hz, 6H, H^{α}/C_5H_4). $^{13}C\{^1H\}$ NMR (δ, $CDCl_3$): 62.3 (C^i/C_5H_4), 70.5 (C^{β}/C_5H_4), 70.7 (C_5H_5), 72.8 (C^{α}/C_5H_4), 109.7 (C≡C). $^{31}P\{^1H\}$ NMR (δ, $CDCl_3$): −66.8.

4.9. Synthesis of [(FcC≡C)Ph_2PAuCl] (**8a**)

To a tetrahydrofuran solution (30 mL) containing 240 mg (0.75 mmol) of [(tht)AuCl] (**7**) was added dropwise a solution with 283 mg (1.132 mmol) of (FcC≡C)Ph_2P (**1a**) in 30 mL of tetrahydrofuran over a period of 1 h at 0 °C. After 1 h of stirring at 25 °C, all volatiles were removed in *oil-pump* vacuum. The title compound was chromatographed on silica gel with diethyl ether as eluent. Compound **8a** was isolated as an orange solid. Yield: 350 mg (0.73 mmol, 97% based on **7**).

Anal. Calc. for $C_{24}H_{19}AuClFeP$ (625.99): C, 46.01; H, 3.06. Found: C, 45.97; H, 3.17%. M.p.: 181 °C (decomp.). IR (KBr, cm^{-1}): 2158 (s, $\nu_{C\equiv C}$). ^1H NMR (δ, $CDCl_3$): 4.25 (s, 5H, C_5H_5), 4.37 (pt, J_{HH} = 1.9 Hz, 2H, H^{β}/C_5H_4), 4.63 (pt, J_{HH} = 1.9 Hz, 2H, H^{α}/C_5H_4), 7.44–7.58 (m, 6H, C_6H_5), 7.75–7.88 (m, 4H, C_6H_5). $^{13}C\{^1H\}$ NMR (δ, $CDCl_3$): 60.6 (d, J_{CP} = 3.8 Hz, C^i/C_5H_4), 70.6 (C_5H_5), 70.6 (C^{β}/C_5H_4), 72.8 (d, J_{CP} = 1.4 Hz, C^{α}/C_5H_4), 112.5 (d, J_{CP} = 22.8 Hz, C≡C), 129.4 (d, J_{CP} = 13.0 Hz, C^m/C_6H_5), 129.8 (d, J_{CP} = 71.0 Hz, C^i/C_6H_5), 132.2 (d, J_{CP} = 2.9 Hz, C^p/C_6H_5), 133.0 (d, J_{CP} = 15.8 Hz, C^o/C_6H_5). $^{31}P\{^1H\}$ NMR (δ, $CDCl_3$): 1.9.

4.10. Synthesis of [((FcC≡C)$_2$PhP)AuCl] (**8b**)

To a tetrahydrofuran solution (30 mL) containing 526 mg (1.00 mmol) of $(FcC\equiv C)_2PhP$ (**1b**) in 30 mL were added 240 mg (0.75 mmol) of [(tht)AuCl] (**7**) dissolved in 30 mL of tetrahydrofuran over a period of 1 h at 0 °C. After appropriate work-up (see **8a**), the title compound was column chromatographed on silica gel using diethyl ether as eluent. Complex **8b** could be obtained as an orange solid. Yield: 486 mg (0.64 mmol, 86% based on **7**).

Anal. Calc. for $C_{30}H_{23}AuClFe_2P$ (757.96): C, 47.50; H, 3.06. Found: C, 47.80; H, 3.21%. M.p.: 93 °C. IR (KBr, cm^{-1}): 2154 (s, $\nu_{C\equiv C}$). ^1H NMR (δ, $CDCl_3$): 4.26 (s, 10H, C_5H_5), 4.33 (pt, J_{HH} = 1.9 Hz, 4H, H^{β}/C_5H_4), 4.59 (pt, J_{HH} = 1.6 Hz, 4H, H^{α}/C_5H_4), 7.50–7.58 (m, 3H, C_6H_5), 7.91–8.03 (m, 2H, C_6H_5). $^{13}C\{^1H\}$ NMR (δ, $CDCl_3$): 61.2 (d, J_{CP} = 2.9 Hz, C^i/C_5H_4), 70.4 (C^{β}/C_5H_4), 70.5 (C_5H_5), 72.7 (d, J_{CP} = 4.8 Hz, C^{α}/C_5H_4), 75.4 (C≡C), 109.2 (d, J_{CP} = 24.3 Hz, C≡C), 129.4 (d, J_{CP} = 12.8 Hz, C^m/C_6H_5), 129.5 (C^i/C_6H_5), 131.8 (C^p/C_6H_5), 132.4 (d, J_{CP} = 18.3 Hz, C^o/C_6H_5). $^{31}P\{^1H\}$ NMR (δ, $CDCl_3$): −37.5.

4.11. Synthesis of [((FcC≡C)Ph_2P)AuC≡CFc] (**9a**)

To a diethylamine solution (50 mL) containing 150 mg (0.24 mmol) of [((FcC≡C)Ph_2P)AuCl] (**8a**) and 60 mg (0.29 mmol) of ethynylferrocene was added 1 mg of [CuI]. After 2 h stirring at 25 °C all volatiles were removed in *oil-pump* vacuum and **9a** was purified by chromatography on silica gel with a hexane/diethyl ether mixture (1:4, vs/vs) as eluent. Yield: 160 mg (0.20 mmol, 84% based on **8a**).

Anal. Calc. for $C_{36}H_{28}AuFe_2P$ (800.03): C, 54.00; H, 3.53. Found: C, 54.05; H, 3.85%. M.p.: 89 °C. IR (KBr, cm^{-1}): 2157 (s, $\nu_{C\equiv C}$). ^1H NMR (δ, $CDCl_3$): 4.13 (pt, J_{HH} = 1.9 Hz, 2H, H^{β}/AuC≡CFc), 4.22 (s, 5H, C_5H_5/AuC≡CFc), 4.25 (s, 5H, C_5H_5/PC≡CFc), 4.35 (pt, J_{HH} = 1.9 Hz, 2H, H^{β}/PC≡CFc), 4.46 (pt, J_{HH} = 1.9 Hz, 2H, H^{α}/AuC≡CFc), 4.61 (pt, J_{HH} = 1.9 Hz, 2H, H^{α}/PC≡CFc), 7.42–7.54 (m, 6H, C_6H_5), 7.77–7.90 (m, 4H, C_6H_5). $^{13}C\{^1H\}$ NMR (δ, $CDCl_3$): 61.1 (d, J_{CP} = 3.0 Hz, C^i/C_5H_4/PC≡CFc), 67.4 (C^i/C_5H_4/AuC≡CFc), 68.0 (C_5H_4/AuC≡CFc), 70.2 (C_5H_5/AuC≡CFc), 70.4 (C_5H_4/AuC≡CFc),

Table 6
Crystal and Intensity Collection Data for **3c**, **5** and **6**.

	3c	5	6
Formula weight	1709.57	1486.52	674.10
Chemical formula	$C_{72}H_{54}Cl_2Fe_6P_2Pt$ 1.5 CH_2Cl_2	$C_{72}H_{56}Fe_4P_2Pt$ CH_2Cl_2	$C_{36}H_{27}Fe_3OP$
Crystal system	Triclinic	Triclinic	Monoclinic
Space group	$P\bar{1}$	$P\bar{1}$	$P2_1/c$
a (Å)	12.9786(10)	8.1907(6)	12.5325(7)
b (Å)	15.7926(11)	11.9938(7)	11.9733(8)
c (Å)	16.5193(15)	16.4187(10)	18.7893(15)
α (°)	96.071(7)	72.625(5)	
β (°)	106.794(7)	79.284(6)	103.321(6)
γ (°)	96.893(6)	74.838(6)	
V (Å^3)	3182.7(4)	1475.54(16)	2743.6(3)
ρ_{calc} (g cm^{-3})	1.784	1.673	1.632
$F(000)$	1694	742	1376
Crystal dimensions (mm)	0.05 × 0.02 × 0.02	0.4 × 0.1 × 0.02	0.3 × 0.1 × 0.1
Z	2	1	4
Maximum and minimum Transmission	1.00000, 0.86690	1.00000, 0.84829	1.01231, 0.98667
Absorption coefficient (λ, mm^{-1})	3.823	3.511	1.654
Scan range (°)	2.88–26.07	3.28–26.06	2.99–26.00
Index ranges	$-16 \le h \le 16$, $-19 \le k \le 19$, $-20 \le l \le 20$	$-10 \le h \le 10$, $-14 \le k \le 14$, $-20 \le l \le 20$	$-15 \le h \le 15$, $-14 \le k \le 14$, $-23 \le l \le 23$
Total reflections	31935	14372	26684
Unique reflections	12570	5783	5393
R_{int}	0.0438	0.0388	0.0229
Data/restraints/parameters	12570/0/793	5783/12/397	5393/0/370
Goodness-of-fit on F^2	0.933	0.977	1.032
R_1[a], wR_2[a] [I 2$\sigma(I)$]	0.0310, 0.0507	0.0288, 0.0528	0.0221, 0.0585
R_1[a], wR_2[a] (all data)	0.0551, 0.0573	0.0416, 0.0580	0.0282, 0.0602
Largest difference peak and hole (e Å^{-3})	1.802, −1.298	1.295, −0.848	0.357, −0.499

[a] $R_1 = [\Sigma(||F_o| - |F_c||)/\Sigma|F_o|)$; $wR_2 = [\Sigma(w(F_o^2 - F_c^2)^2)/\Sigma(wF_o^4)]^{1/2}$. $S = [\Sigma w(F_o^2 - F_c^2)^2]/(n - p)^{1/2}$. n = number of reflections, p = parameters used.

Table 7
Crystal and intensity collection data for **8a**, **9a**, and **9b**.

	8a	9a	9b
Formula weight	626.63	800.22	905.12
Chemical formula	$C_{24}H_{19}AuClFeP$	$C_{36}H_{28}AuFe_2P$	$C_{36}H_{28}AuFePRu$ 0.5 $CHCl_3$
Crystal system	Monoclinic	Monoclinic	Monoclinic
Space group	$P2_1/n$	$P2_1/c$	$P2_1/a$
a (Å)	9.9198(7)	15.3726(17)	13.7289(10)
b (Å)	19.1756(15)	7.5512(5)	18.3090(13)
c (Å)	12.0771(9)	24.927(3)	14.4577(8)
β (°)	113.071(7)	106.505(10)	114.223(6)
V (Å^3)	2113.5(3)	2774.3(5)	3314.2(4)
ρ_{calc} (g cm^{-3})	1.969	1.916	1.814
$F(000)$	1200	1560	1748
Crystal dimensions (mm)	0.5 × 0.2 × 0.1	0.5 × 0.2 × 0.1	0.3 × 0.2 × 0.05
Z	4	4	4
Maximum and minimum Transmission	1.47670, 0.34621	1.19314, 0.68665	1.00000, 0.46972
Absorption coefficient (λ, mm^{-1})	7.829	6.390	5.491
Scan range (°)	3.08–26.08	4.90–25.50	2.97–26.09
Index ranges	$-12 \le h \le 12$, $-23 \le k \le 23$, $-14 \le l \le 14$	$-18 \le h \le 18$, $-8 \le k \le 9$, $-30 \le l \le 30$	$-16 \le h \le 16$, $-22 \le k \le 22$, $-17 \le l \le 17$
Total reflections	20397	17054	32220
Unique reflections	4171	5026	6536
R_{int}	0.0286	0.0276	0.0349
Data/restraints/parameters	4171/0/253	5026/15/361	6536/41/394
Goodness-of-fit on F^2	1.055	1.045	1.102
R_1[a], wR_2[a] [I $2\sigma(I)$]	0.0165, 0.0384	0.0258, 0.0598	0.0384, 0.1090
R_1[a], wR_2[a] (all data)	0.0216, 0.0393	0.0299, 0.0610	0.0548, 0.1152
Largest difference peak and hole (e Å^{-3})	0.848, −0.727	3.073, −1.151	3.845, −1.583

[a] $R_1 = [\Sigma(||F_o| - |F_c|)/\Sigma|F_o|]$; $wR_2 = [\Sigma(w(F_o^2 - F_c^2)^2)/\Sigma(wF_o^4)]^{1/2}$. $S = [\Sigma w(F_o^2 - F_c^2)^2]/(n - p)^{1/2}$. n = number of reflections, p = parameters used.

70.5 (C_5H_5/PC≡CFc), 72.0 ($C^{\beta}C_5H_4$/PC≡CFc), 72.7 (d, J_{CP} = 1.0 Hz, C^{α}/C_5H_4/PC≡CFc), 129.3 (d, J_{CP} = 12.5 Hz, C^{m}/C_6H_5), 130.8 (d, J_{CP} = 63.3 Hz, C^{i}/C_6H_5), 131.8 (d, J_{CP} = 2.4 Hz, C^{p}/C_6H_5), 133.2 (d, J_{CP} = 15.8 Hz, C^{o}/C_6H_5). $^{31}P\{^1H\}$ NMR (δ, $CDCl_3$): 15.1.

4.12. Synthesis of [((FcC≡C)Ph_2P)AuC≡CRc] (9b)

Complex **9b** was synthesized in a similar manner as discussed for **9a**: 150 mg (0.24 mmol) of [((FcC≡C)Ph_2P)AuCl] (**8**) were reacted with 80 mg (0.31 mmol) of ethynyl ruthenocene at 50 °C. After appropriate work-up, compound **9b** was isolated as an orange–yellow solid. Yield: 180 mg (0.21 mmol, 89%).

Anal. Calc. for $C_{36}H_{28}AuFePRu \times CH_2Cl_2$ (930.93): C, 47.74; H, 3.25. Found: C, 48.18; H, 3.25%. M.p.: 95 °C. IR (KBr, cm^{-1}): 2167 (s, $\nu_{C\equiv C}$). ^1H NMR (δ, $CDCl_3$): 4.24 (s, 5H, C_5H_5/Fc), 4.35 (pt, J_{HH} = 1.7 Hz, 2H, H^{β}/Fc), 4.49 (pt, J_{HH} = 1.7 Hz, 2H, H^{β}/Rc), 4.59–4.61 (m, 2H, H^{α}/Fc; 5H, C_5H_5/Rc), 4.88 (pt, J_{HH} = 1.7 Hz, 2H, H^{α}/Rc), 5.29 (CH_2Cl_2) 7.41–7.56 (m, 6H, C_6H_5), 7.76–7.88 (m, 4H, C_6H_5). $^{13}C\{^1H\}$ NMR (δ, $CDCl_3$): 70.0 (C_5H_4/Rc), 70.4 ($C^{\beta}C_5H_4$/Fc), 70.5 (C_5H_5/Fc), 71.9 (C_5H_5/Rc), 72.7 (d, J_{CP} = 1.0 Hz, C^{α}/C_5H_4/Fc), 74.4 (C_5H_4/Rc), 129.3 (d, J_{CP} = 12.5 Hz, C^{m}/C_6H_5), 130.8 (d, J_{CP} = 64.3 Hz, C^{i}/C_6H_5), 131.8 (C^{p}/C_6H_5), 133.2 (d, J_{CP} = 15.4 Hz, C^{o}/C_6H_5). $^{31}P\{^1H\}$ NMR (δ, $CDCl_3$): 14.9.

5. Crystal structure determinations

Crystal and intensity collection data for **3c**, **5**, **6**, **8a**, **9a**, and **9b** are summarized in Table 6 (**3c**, **4**, and **6**) and Table 7 (**8a**, **9a**, and **9b**). All data were collected on a Oxford Gemini S diffractometer with graphite monochromatized Mo Kα radiation (λ = 0.71073 Å) at 100 K (**4**, **6**, **8a**, **9a**, and **9b**) and Cu Kα radiation (λ = 1.54 Å) at 110 K (**3c**) using oil-coated shock-cooled crystals [50]. The structures were solved by direct methods using SHELXS-97 [51] and SIR-92 (**3c**) [53] and refined by full-matrix least-square procedures on F^2 using SHELXL-97. [52] All *non*-hydrogen atoms were refined anisotropically and a riding model was employed in the refinement of the hydrogen atom positions.

Supplementary material

CCDC 697272, 697273, 697271, 697269, 697268 and 697270 contain the supplementary crystallographic data for **3c**, **5**, **6**, **8a**, **9a** and **9b**. These data can be obtained free of charge from The Cambridge Crystallographic Data Centre via http://www.ccdc.cam.ac.uk/data_request/cif.

Acknowledgement

We are grateful to the Deutsche Forschungsgemeinschaft and the Fonds der Chemischen Industrie for financial support. Catharina Meier is acknowledged for fruitful discussions.

References

[1] (a) M.I. Bruce, P.A. Humphrey, M. Jevric, G.J. Perkins, B.W. Skelton, A.H. White J. Organomet. Chem. 692 (2007) 1748;
(b) J. Durand, S. Gladiali, G. Erre, E. Zangrando, B. Milani, Organometallics 26 (2007) 810;
(c) R.C.J. Atkinson, K. Gerry, V.C. Gibson, N.J. Long, E.L. Marshall, L.J. West, Organometallics 26 (2007) 316;
(d) P. Debroy, S. Roy, Coord. Chem. Rev. 251 (2007) 203;
(e) T.Y. Dong, M. Lin, M.Y.N. Chiang, J.Y. Wu, Organometallics 23 (2004) 3921;
(f) T.Y. Dong, K. Chen, M.C. Lin, L. Lee, Organometallics 24 (2005) 4198;
(g) N.J. Long, Angew. Chem., Int. Ed. 34 (1995) 21;
(h) Special issue, "50th Anniversary of the Discovery of Ferrocene", J. Organomet. Chem. 637–639 (2001), (R.D. Adams, Ed.), and references therein.
[2] (a) C.P. Berlinguette, K.R. Dumbar, Chem. Commun. (2005) 2451;
(b) S. Santi, L. Orian, A. Donoli, C. Durante, A. Bisello, P. Ganis, A. Ceccon, Organometallics 26 (2007) 5867;
(c) K. Heinze, S. Reinhardt, Organometallics 26 (2007) 5406;
(d) S. Rabaça, I.C. Santos, M.T. Duarte, V. Gama, Inorg. Chim. Acta 360 (2007) 3855.
[3] (a) F. Barrière, R.U. Kirss, W.E. Geiger, Organometallics 24 (2005) 48;
(b) A. Shafir, M.P. Power, G.D. Whitener, J. Arnold, Organometallics 19 (2000) 3978;
(c) A. Mendiratta, S. Barlow, M.W. Day, S.R. Marder, Organometallics 18 (1999) 454.
[4] (a) M.I. Bruce, Coord. Chem. Rev. 248 (2004) 1603;
(b) S. Szafert, J.A. Gladysz, Chem. Rev. 106 (2006) PR1;
(c) C. Lapinte, J. Organomet. Chem. 693 (2008) 793;
(d) H. Lang, D.S.A. George, G. Rheinwald, Coord. Chem. Rev. 206–207 (2000) 101;

(e) P.J. Low, Annu. Rep. Prog. Chem. Sect. A 102 (2006) 379;
(f) K. Venkatesan, O. Blacque, H. Berke, Dalton Trans. (2007) 1091;
(g) H. Lang, R. Packheiser, Collect. Czech. Chem. Commun. 72 (2007) 435;
(h) H. Lang, A. Jakob, Organometallic Chemistry Research Perspectives, in: Richard P. Irwin (Ed.), Nova Science Publishers Inc., 2007, p. 99;
(i) N.J. Long, C.K. Williams, Angew. Chem., Int. Ed. 42 (2003) 2586;
(j) K.-L. Cheung, S.-K. Yip, V.W.-W. Yam, J. Organomet. Chem. 689 (2004) 4451;
(k) K.-C. Cheung, W.-L. Wong, D.-L. Ma, T.-S. Lai, K.-Y. Wong, Coord. Chem. Rev. 251 (2007) 2367;
(l) T.-Y. Dong, M.-C. Lin, M. Y.-N. Chiang, J.-Y. Wu, Organometallics 23 (2004) 3921;
(m) M.P. Cifuentes, M.G. Humphrey, J. Organomet. Chem. 689 (2004) 3968;
(n) B. Bildstein, Coord. Chem. Rev. 206–207 (2000) 369;
(o) R. Packheiser, P. Ecorchard, T. Rüffer, H. Lang, Organometallics 27 (2008) 3534;
(p) T. Baumgartner, R. Réau, Chem. Rev. 106 (2006) 4681;
(q) R. Malacea, E. Manoury, L. Routaboul, J.-C. Daran, R. Poli, J.P. Dunne, A.C. Withwood, C. Godard, S.B. Duckett, Eur. J. Inorg. Chem. (2006) 1803;
(r) P. Teo, D.M.J. Foo, L.L. Koh, T.S.A. Hor, Dalton Trans. (2004) 3389;
(s) P.M.N. Low, A.L. Tan, T.S.A. Hor, Y.-S. Wen, L.-K. Liu, Organometallics 15 (1996) 2595;
(t) W. Weigand, C. Robl, Chem. Ber. 126 (1993) 1807.

[5] (a) T. Baumgartner, M. Fiege, F. Pontzen, R. Arteaga-Müller, Organometallics 25 (2006) 5657;
(b) A. Jakob, B. Milde, P. Ecorchard, C. Schreiner, H. Lang, J. Organomet. Chem. (2008). doi: 0.1016/j.jorganchem.2008.09.040;
(c) P. Low, J. Clust. Sci. 19 (2008) 5.

[6] (a) G.K. Anderson, H.C. Clark, J.A. Davis, G. Ferguson, M. Parvez, J. Crystallogr. Spectrosc. Res. 12 (1982) 449;
(b) P.M. Van Calcar, M.M. Olmstead, A.L. Balch, Chem. Commun. (1996) 2597;
(c) K. Mikami, H. Kakuno, K.A. Kawa, Angew. Chem., Int. Ed. 44 (2005) 7423.

[7] (a) A. Hengefeld, J. Kopf, D. Rehder, Organometallics 2 (1983) 114;
(b) E.C. Constable, C.E. Housecroft, B. Krattinger, M. Neuburger, M. Zehnder, Organometallics 18 (1999) 2565;
(c) D.K. Johnson, T. Rukachaisirikul, Y. Sun, N.J. Taylor, A.J. Canty, A.J. Carty, Inorg. Chem. 32 (1993) 5544.

[8] R. Packheiser, B. Walfort, H. Lang, Oranometallics 25 (2006) 4579.

[9] A.D. Burrows, D.M.P. Mingos, S.E. Lawrence, A.J.P. White, D.J. Williams, J. Chem. Soc., Dalton Trans. (1997) 1295.

[10] (a) K. Gagnon, S.M. Aly, A. Brisach-Wittmeyer, D. Bellows, J.-F. Bérubé, L. Caron, A.S. Abd-El-Aziz, D. Fortin, P.D. Harvey, Organometallics 27 (2008) 2201;
(b) E. Robé, C. Hegedüs, J. Bakos, Y. Coppel, J.-C. Daran, M. Gouygou, Inorg. Chim. Acta 361 (2008) 1861;
(c) T. Cardolaccia, Y. Li, K.S. Schanze, J. Am. Chem. Soc. 130 (2008) 2535;
(d) A. Sivaramakrishna, B.C.E. Makhubela, F. Zheng, H. Su, G.S. Smith, J.R. Moss, Polyhedron 27 (2008) 44;
(e) J. Forniés, M.A. Gómez-Saso, E. Lallnde, F. Martinez, M.T. Moreno, Organometallics 11 (1992) 2873;
(f) K. Sonogashira, Y. Fujikura, T. Yatake, N. Toyoshima, S. Takahashi, N. Hagihara, J. Organomet. Chem. 145 (1978) 101;
(g) S. Takahashi, Y. Takai, H. Morimoto, K. Sonogashira, N. Hagihara, Mol. Cryst. Liq. Cryst. 82 (1982) 139;
(h) K. Sonogashira, T. Yatake, Y. Tohda, S. Takahashi, N. Hagihara, J. Chem. Soc., Chem. Commun. (1977) 291;
(i) K. Sonogashira, S. Takahashi, N. Hagihara, Macromolecules (1977) 879;
(j) I. Collimati, A. Furlani, J. Organomet. Chem. 17 (1969) 457;
(k) R.J. Cross, M.F. Davidson, J. Chem. Soc., Dalton Trans. (1986) 1987.

[11] R.J. Cross, I.G. Phillips, J. Chem. Soc., Dalton Trans. (1982) 2261.

[12] (a) M. Carlsson, B. Eliasson, Organometallics 25 (2006) 5500;
(b) R. D'Amato, A. Furlani, M. Colapietro, G. Portalone, M. Casalboni, M. Falconieri, M.V. Russo, J. Organomet. Chem. 627 (2001) 13.

[13] R.F. De Ketellaere, G.P. van der Kelen, J. Mol. Struct. 23 (1974) 233.

[14] (a) G. Bandoli, G. Bortolozzo, D.A. Clemente, U. Croatto, C. Panettoni, J. Chem. Soc. (A) Inorg. Phys. Theor. (1970) 2778;
(b) C.M. Whitaker, K.L. Kott, R.J. McMahon, J. Org. Chem. 60 (1995) 3499.

[15] J. Vicente, M.T. Chicote, M.T. Abrisqueta, J.G. Jones, Organometallics 16 (1997) 5628.

[16] H. Lang, S. Köcher, S. Back, G. Rheinwald, G. van Koten, Organometallics 20 (2001) 1968.

[17] N.C. Baenziger, W.E. Bennett, D.M. Soboroff, Acta Crystallogr. B 32 (1976) 962.

[18] (a) K. Rößler, T. Rüffer, B. Walfort, R. Packheiser, R. Holze, M. Zharnikov, H. Lang, J. Organomet. Chem. 692 (2007) 1530;
(b) T.J. Burchell, M.C. Jennings, R.J. Puddephatt, Inorg. Chim. Acta 359 (2006) 2812.

[19] R. Packheiser, A. Jakob, P. Ecorchard, B. Walfort, H. Lang, Organometallics 27 (2008) 1214.

[20] G. Gritzner, J. Kuta, Pure Appl. Chem. 56 (1984) 461.

[21] H. Strehlow, W. Knoche, H. Schneider, Ber. Bunsen. Phys. Chem. 77 (1973) 760.

[22] (a) T. Kuwana, D.E. Bublitz, G. Hoh, J. Am. Chem. Soc. 82 (1960) 5811;
(b) S.P. Gubin, S.A. Smirnova, L.I. Denisovich, A.A. Lubovich, J. Organomet. Chem. 30 (1971) 243;
(c) S.V. Kukharenko, V.V. Strelets, A.R. Kudinov, A.Z. Kreitlin, M.G. Peterleitner, L.I. Denisovich, M.I. Rybinskaya, J. Organomet. Chem. 519 (1996) 1.

[23] (a) Reversible oxidation to the ruthenocenium radical cation and its equilibrium with the dimeric $[Cp_2Ru–RuCp_2]^{2+}$ dication has been reported in less nucleophilic environments M.G. Hill, W.M. Lamanna, K.R. Mann, Inorg. Chem. 30 (1991) 4690;
(b) S. Trupia, A. Nafady, W.E. Geiger, Inorg. Chem. 42 (2003) 5480.

[24] Instrumental Methods in Electrochemistry, The Southampton Electrochemical Group, Horwood Publishing, Chichester, 2001 (Chapter 6.3.2).

[25] M. Sato, Y. Kubota, Y. Kawata, T. Fujihara, K. Unoura, A. Oyama, Chem. Eur. J. 12 (2006) 2282.

[26] M. Sato, A. Iwai, M. Watanabe, Organometallics 18 (1999) 3208.

[27] M. Sato, Y. Kawata, H. Shintate, Y. Habata, S. Akabori, K. Unoura, Organometallics 16 (1997) 1693.

[28] M. Sato, H. Shintate, Y. Kawata, M. Sekino, M. Katada, S. Kawata, Organometallics 13 (1994) 1956.

[29] M.C.B. Colbert, S.L. Ingham, J. Lewis, N.J. Long, P.R. Raithby, J. Chem. Soc., Dalton Trans. (1994) 2215.

[30] M. Sato, E. Mogi, M. Katada, Organometallics 14 (1995) 4837.

[31] S. Back, R.A. Gossage, H. Lang, G. van Koten, Eur. J. Inorg. Chem. (2000) 1457.

[32] M. Sato, Y. Hayashi, H. Shintate, M. Katada, S. Kawata, J. Organomet. Chem. 471 (1994) 179.

[33] N.J. Long, A.J. Martin, A.J.P. White, D.J. Williams, M. Fontani, F. Laschi, P. Zanello, J. Chem. Soc., Dalton Trans. (2000) 3387.

[34] M.C.B. Colbert, J. Lewis, N.J. Long, P.R. Raithby, A.J.P. White, D.J. Williams, J. Chem. Soc., Dalton Trans. (1997) 99.

[35] N.D. Jones, M.O. Wolf, D.M. Giaquinta, Organometallics 16 (1997) 1352.

[36] Y. Zhu, O. Clot, M.O. Wolf, G.P.A. Yap, J. Am. Chem. Soc. 120 (1998) 1812.

[37] G. Vives, A. Carella, J.-P. Launay, G. Rapenne, Chem. Commun. (2006) 2283.

[38] (a) D. Osella, O. Gambino, C. Nervi, M. Ravera, M.V. Russo, G. Infante, Inorg. Chim. Acta 225 (1994) 35;
(b) D. Osella, R. Gobetto, C. Nervi, M. Ravera, R. D'Amato, M.V. Russo, Inorg. Chem. Commun. 1 (1998) 239.

[39] M. Sato, Y. Hayashi, S. Kumakura, N. Shimizu, M. Katada, S. Kawata, Organometallics 15 (1996) 721.

[40] C.J. Adams, S.L. James, X. Liu, P.R. Raithby, L.J. Yellowlees, J. Chem. Soc., Dalton Trans. (2000) 63.

[41] M. Ravera, R. D'Amato, A. Guerri, J. Organomet. Chem. 690 (2005) 2376.

[42] E.C. James, M.Jura;G. Kociok-Köhn, P.R. Raithby, E.L. Sharp, P.J. Wilson, Inorg. Chem. 46 (2007) 7232.

[43] Y.-J. Chen, S.-S. Chen, S.-S. Lo, T.-H. Huang, C.-C. Wu, G.-H. Lee, S.-M. Peng, C.-Y. Yeh, Chem. Commun. (2006) 1015.

[44] S.C. Jones, V. Coropceanu, S. Barlow, T. Kinnibrugh, T. Timofeeva, J.-L. Brédas, S.R. Marder, J. Am. Chem. Soc. 126 (2004) 11782.

[45] M. B-Robin, P. Day, Adv. Inorg. Chem. Radiochem. 10 (1967) 247.

[46] M. Krejcik, M. Danek, F. Hartl, J. Electroanal. Chem. 317 (1991) 179.

[47] (a) J. Polin, H. Schottenberger, Org. Syn. 73 (1996) 262;
(b) M.O. Rausch, A. Siegel, J. Org. Chem. 34 (1969) 1974.

[48] H.H. Eysel, E. Guggolz, M. Kopp, M.L. Ziegler, Z. Anorg. Allg. Chem. 499 (1988) 81.

[49] K.C. Dash, H. Schmidbaur, Chem. Ber. 106 (1973) 1221.

[50] (a) T. Kottke, D.J. Stalke, Appl. Crystallogr. 26 (1993) 615;
(b) T. Kottke, R.J. Lagow, D.J. Stalke, Appl. Crystallogr. 29 (1996) 465;
(c) D. Stalke, Chem. Soc. Rev. 27 (1998) 171.

[51] G.M. Sheldrick, Acta Crystallogr. Sect. A 46 (1990) 467.

[52] A. Altomare, G. Cascarano, C. Giacovazzo, A. Gualardi, J. Appl. Cryst. 26 (1993) 343.

[53] G.M. Sheldrick, SHELXL-97, Program for Crystal Structure Refinement, University of Göttingen, 1997.